

# Ice-Nucleating Particles Near Two Major Dust Source Regions

Charlotte M. Beall<sup>1,2</sup>, Thomas C. J. Hill<sup>3</sup>, Paul J. DeMott<sup>3</sup>, Tobias Köneman<sup>2\*</sup>, Michael Pikridas<sup>4</sup>,  
Frank Drewnick<sup>5</sup>, Hartwig Harder<sup>6</sup>, Christopher Pöhlker<sup>2</sup>, Jos Lelieveld<sup>4,6</sup>, Bettina Weber<sup>2\*\*</sup>,  
Minas Iakovides<sup>4</sup>, Roman Prokeš<sup>7,8</sup>, Jean Sciare<sup>4</sup>, Meinrat O. Andreae<sup>1,2,9</sup>, M. Dale Stokes<sup>1</sup>,  
Kimberly A. Prather<sup>1,10</sup>

<sup>1</sup>Scripps Institution of Oceanography, University of California San Diego, La Jolla, CA 92037, USA

<sup>2</sup>Max Planck Institute for Chemistry, Multiphase Chemistry and Biogeochemistry Departments, D-55128 Mainz, Germany

<sup>3</sup>Department of Atmospheric Science, Colorado State University, Fort Collins, CO 80523, USA

<sup>4</sup>Climate & Atmosphere Research Center, The Cyprus Institute, Nicosia, CY-1645, Cyprus

<sup>5</sup>Max Planck Institute for Chemistry, Particle Chemistry Department, D-55128 Mainz, Germany

<sup>6</sup>Max Planck Institute for Chemistry, Atmospheric Chemistry Department, D-55128 Mainz, Germany

<sup>7</sup>RECETOX, Faculty of Science, Masaryk University, Kotlarska 2, 611 Brno, Czech Republic

<sup>8</sup>Department of Atmospheric Matter Fluxes and Long-range Transport, Global Change Research Institute of the Czech Academy of Sciences, Belidla 4a, 60300, Brno, Czech Republic

<sup>9</sup>Department of Geology and Geophysics, King Saud University, Riyadh, Saudi Arabia

<sup>10</sup>Department of Chemistry and Biochemistry, University of California San Diego, La Jolla, CA, 92093 USA

\*Now at Envicontrol GmbH, Waidmarkt 11, 50676 Köln, Germany

\*\*Now at: Institute of Biology, University of Graz, 8010 Graz, Austria

32 Correspondence to: Charlotte M. Beall, [cbeall@ucsd.edu](mailto:cbeall@ucsd.edu)

### 33 **Abstract**

34 Mineral dust and sea spray aerosol represent important sources of ice-nucleating particles (INPs), the minor  
35 fraction of aerosol particles able to trigger cloud ice crystal formation and, consequently, influence multiple  
36 climate-relevant cloud properties including lifetime, radiative properties and precipitation initiation  
37 efficiency. Mineral dust is considered the dominant INP source in many parts of the world due to its ice  
38 nucleation efficiency and its sheer abundance, with global emission rates of up to 4700 Tg a<sup>-1</sup>. However,  
39 INPs emitted from the ocean surface in sea spray aerosol frequently dominate INP populations in remote  
40 marine environments, including parts of the Southern Ocean where cloud-resolving model simulations have  
41 demonstrated that cloud radiative properties are likely strongly controlled by INPs. Here we report INP  
42 concentrations measured in aerosol and seawater samples during Air Quality and Climate Change in the  
43 Arabian BASin (AQABA), a shipborne campaign that spanned the Red Sea, Gulf of Aden, Arabian Sea,  
44 Arabian Gulf, and part of the Mediterranean. In aerosol samples collected within a few hundred kilometers  
45 of the first and second ranked sources of dust globally, the Sahara and Arabian Peninsula, INP  
46 concentrations ranged from 0.2 to 11 L<sup>-1</sup> at -20 °C with observed ice-active surface site densities ( $n_s$ ) 1-3  
47 orders of magnitude below levels predicted by mineral dust INP parameterizations. Over half of the samples  
48 (at least 14 of 26) were collected during dust storms with average dust mass concentrations between 150  
49 and 490 µg m<sup>-3</sup> (PM<sub>10</sub>), as simulated by the Modern-Era Retrospective analysis for Research and  
50 Application, version 2 (MERRA-2). The impacts of heat and peroxide treatments indicate that organics  
51 dominated the observed ice nucleation (IN) -activity at temperatures  $\geq$  -15 °C with proteinaceous (heat-  
52 labile) INPs frequently observed at high freezing temperatures  $>$  -10 °C. INP concentrations in seawater  
53 samples ranged between 3 and 46 mL<sup>-1</sup> at -19 °C, demonstrating the relatively low INP source potential of  
54 seawater in the region as compared to seawater from multiple other regions reported previously. Overall,  
55 our results demonstrate that despite proximity to the Sahara and the Arabian Peninsula and the dominance  
56 of mineral dust in the aerosol sampled, existing mineral dust parameterizations alone would not skillfully  
57 represent the near-surface  $n_s$  in the observed temperature regime (-6 to -25 °C). Future efforts to develop  
58 or improve representations of dust INPs at modest supercooling ( $\geq$ -15 °C) would benefit from a  
59 characterization of the specific organic species associated with dust INPs. More generally, an improved  
60 understanding of the organic species associated with increased IN -activity and their variability across dust  
61 source regions would directly inform efforts to determine whether  $n_s$ -based parameterizations are  
62 appropriate for faithful representation of dust INPs in this sensitive temperature regime, whether region-  
63 specific parameterizations are required, or whether an alternative to the  $n_s$  approach is necessary.

## 64 **1 Introduction**

65 Ice-nucleating particles (INPs) modulate the temperature and relative humidity at which ice  
66 particle formation occurs in the atmosphere and thus are a key factor that controls ice-phase  
67 partitioning in clouds. As initiators of ice formation and related phase-partitioning processes, INPs  
68 affect multiple cloud properties and exert a strong influence on cloud lifetime, radiative properties  
69 and precipitation initiation efficiency (e.g. Lohmann and Feichter, 2005; Vergara-Temprado et al.,  
70 2018; Brunner et al., 2021).

71 Globally, desert dust is likely the most abundant aerosol type by mass (Kinne et al., 2006; Kok et  
72 al., 2021). Furthermore, multiple studies have demonstrated that mineral dust is the dominant ice-  
73 nucleating species in many parts of the world based on observations (Ardon-Dryer and Levin,  
74 2014; Boose et al., 2016; DeMott et al., 2015a; Price et al., 2018) and modeling of global INP  
75 distributions (Burrows et al., 2013; Hoose et al., 2010; Murray et al., 2012; Vergara-Temprado et  
76 al., 2017). Annual global dust emission rate estimates range between 400 and 4700 Tg a<sup>-1</sup> (Huneeus  
77 et al., 2011; Kok et al., 2021). Of the average global dust loading in the atmosphere (20-29 Tg),  
78 North African source regions are estimated to contribute ~50% (11-15 Tg), and the Middle East  
79 and Central Asian source regions account for the bulk of the remainder, ~30% (7.7 Tg) (Kok et  
80 al., 2021). Analysis of satellite products indicates that dust emission rates are increasing over the  
81 Middle East at a rate of 15% a<sup>-1</sup> (Klingmüller et al., 2016; Yu et al., 2018).

82 While Hoose and Möhler (2012) showed that mineral dust INPs generally activate ice crystals at  
83 freezing temperatures < -15 °C, dust containing K-feldspar has been shown to nucleate ice at much  
84 warmer temperatures, up to -4 °C (Atkinson et al., 2013; Harrison et al., 2016; Niedermeier et al.,  
85 2015; Wex et al., 2014; Whale et al., 2015; Zolles et al., 2015). K-feldspars represent up to ~24%  
86 of Saharan and Asian dusts by mass (Nickovic et al., 2012). However, knowledge of the abundance  
87 and the available surface fraction of aerosolized K-feldspar would be necessary to evaluate the IN  
88 efficiency of dust at temperatures > -15 °C (Kanji et al., 2017).

89 Though mineral dust is considered to be the dominant INP source in many regions, multiple  
90 modeling and observational studies suggest that marine INPs are frequently dominant by number  
91 in remote ocean regions in air masses with low concentrations of terrestrial aerosol (McCluskey et  
92 al., 2018b, 2018c; Vergara-Temprado et al., 2017; Wilson et al., 2015; DeMott et al., 2016). Using

93 a global aerosol model to simulate marine organic and K-feldspar INP populations, Vergara-  
94 Temprado et al. (2017) showed that the relative contribution of marine organic vs. dust INPs in  
95 remote regions varies seasonally, and that marine organic INPs frequently outnumber K-feldspar  
96 INPs (up to 100% of the simulated days in the Southern Ocean during summer). Results from a  
97 follow-on cloud-resolving model study showed that Southern Ocean cloud reflectivity is strongly  
98 modulated by INP concentrations, indicating that accurate estimates of the radiative energy budget  
99 in the Southern Ocean likely require improved and reliable representation of both dust and marine  
100 organic INPs (Vergara-Temprado et al., 2018). By generating isolated nascent sea spray aerosol  
101 over a range of biological conditions, mesocosm studies have shown that marine INPs are  
102 comprised of two classes: a dissolved organic carbon (DOC) type composed of IN-active  
103 molecules and a particulate organic carbon (POC) type linked to the death phase of phytoplankton  
104 blooms (McCluskey et al., 2017, 2018b).

105 Parameterizations for both marine and mineral dust populations are commonly implemented in  
106 atmospheric models to estimate dust and marine INP concentrations. There are multiple existing  
107 mineral dust INP parameterizations used to estimate their concentrations in aerosolized desert dust,  
108 some based exclusively on laboratory measurements (e.g., Niemand et al., 2012; Ullrich et al.,  
109 2017), and others derived from a combination of laboratory and field measurements (DeMott et  
110 al., 2015). There are, additionally, multiple mineral-specific INP parameterizations including illite  
111 (Broadley et al., 2012), kaolinite (Welti et al., 2012), quartz (Harrison et al., 2019) and K-feldspar  
112 (Atkinson et al., 2013; hereafter, "A13"). The parameterizations by Ullrich et al. (2017; hereafter,  
113 "U17") and Niemand et al. (2012; hereafter, "N12") were developed using dust samples from  
114 multiple deserts, and both found little variability in the IN activity between dusts from locations  
115 as disparate as the Sahara and Asia. DeMott et al. (2015; hereafter, "D15") found agreement  
116 between their observations-based parameterization and N12, supporting the validity of laboratory-  
117 based parameterizations. Results in D15 also confirmed the conclusions of N12 and U17: that to  
118 first order, dusts from distinct regions can be parameterized as a single particle type. The D15  
119 parameterization has been considered to be representative of dust that has undergone atmospheric  
120 photochemical and oxidative processes in transport (i.e., "aged" dust), because the  
121 parameterization was derived from observations made far (1000s of kilometers) from the dust  
122 emissions sources (Boose et al., 2016).

123 By contrast, few studies report *in situ* INP measurements near (e.g., < 1 day of transport) a major  
124 dust source, and the lack of observations near dust source regions inhibit the evaluation of the  
125 ability of existing dust INP parameterizations to represent nascent dust populations (Boose et al.,  
126 2016; Gong et al., 2020; Price et al., 2018). INP observations are particularly lacking for the  
127 sensitive temperature regime > -20 °C. Boose et al. (2016) found that D15 overpredicted INPs  
128 observed during Saharan dust events at a location within 100s of km west of the Sahara (Izaña,  
129 Tenerife, Spain) by 2-3 orders of magnitude, suggesting that aging may lead to increased IN  
130 efficiency in mineral dust and that D15 may be less representative of nascent dust. These  
131 conclusions were supported by Conen et al. (2015), who found that concentrations of INPs at -20  
132 °C measured during Saharan dust events were one order of magnitude higher at Jungfraujoch in  
133 the Swiss Alps than in Izaña, where dust events had occurred 1-7 d prior to reaching Jungfraujoch.  
134 Gong et al. (2020) measured INPs in a variety of atmospheric and seawater sample types at Cabo  
135 Verde and determined mineral dust to be the dominant source of INPs observed in the atmosphere  
136 but found that INPs with freezing temperatures > -10 °C were likely biological. At altitudes  
137 between 30 and 3500 m in the same region, Price et al. (2018) found that measured concentrations  
138 of INPs ranged two orders of magnitude at a given temperature, and that the observed  
139 concentrations related to the atmospheric dust loadings.

140 Recently, multiple studies have provided new, much-needed observations of ambient atmospheric  
141 INPs in marine environments (DeMott et al., 2016; Hartmann et al., 2020; McCluskey et al., 2018c,  
142 2018d; Yang et al., 2020) where data was historically lacking and, consequently, an impediment  
143 to achieving predictive understanding of global INP distributions (Burrows et al., 2013). There  
144 are now two parameterizations available for the estimation of atmospheric concentrations of  
145 marine INPs emitted from the ocean surface: Wilson et al. (2015), which estimates cumulative  
146 INPs from total organic carbon (TOC) concentrations in simulated sea spray aerosol (SSA), and  
147 McCluskey et al. (2018), which estimates ice-active surfacesite density ( $n_s$ ) from aerosol surface  
148 area. Wilson et al. (2015) and McCluskey et al. (2018; hereafter “M18”) derived marine INP  
149 parameterizations from field measurements of INPs in Atlantic and Arctic Ocean sea surface  
150 microlayer samples and pristine SSA samples over the North Atlantic Ocean, respectively.

151 Here, we report observations of INPs measured in air masses influenced by both desert dust and  
152 marine aerosol (Edtbauer et al., 2020) in close proximity to the two greatest global dust aerosol

153 sources: the Sahara (#1) and the Arabian Peninsula (#2) (Kok et al., 2021). INP concentrations  
154 were measured in 26 ambient aerosol samples collected during Air Quality and Climate Change  
155 in the Arabian Basin (AQABA), a shipborne campaign which took place July – August 2017 on a  
156 transect that spanned the central and eastern parts of the Mediterranean, the Red Sea, the Gulf of  
157 Aden, the Arabian Sea and the Arabian Gulf. The rest of this study will be structured as follows.  
158 We present an overview of measurements and data sources in Sect. 2 Methods. In Results Sect.  
159 3.1, an overview of INP concentrations observed is presented, followed by an assessment of  
160 subsurface seawater (SSW) source potential (Sect. 3.2). Observed  $n_s$  are compared to dust and  
161 marine INP parameterizations in Sect. 3.3, followed by an analysis of the contributions of heat-  
162 labile (e.g., proteinaceous) and heat-stable organic compounds to observed INP populations in  
163 aerosol (Sect. 3.4). The same analysis is applied to assess organic contributions to observed INPs  
164 in a soil dust sample from a likely source region in Sect. 3.5. We discuss the findings, potential  
165 INP sources and compare with prior studies in the Discussion Sect. 5. Finally, in Sect. 5 we offer  
166 strategies to address the challenges of evaluating dust-specific INP parameterizations and  
167 recommend measurements needed to develop predictive understanding of dust INPs at modest  
168 supercooling ( $T \geq 15^\circ\text{C}$ ).

## 169 **2 Methods**

### 170 **2.1 Project Overview**

171 The AQABA campaign was conducted from 25 June to 3 September 2017 onboard the RV  
172 *Kommandor Iona*. The research voyage was conducted in two transects: the first leg beginning in  
173 La-Seyne-sur-Mer, France, heading through the Suez Canal, around the Arabian Peninsula and  
174 ending in Kuwait, and second leg a return transect via the same route (Figs. S1-S2). The campaign  
175 supported a large suite of on- and offline aerosol and gas-phase measurements (Bourtsoukidis et  
176 al., 2019, 2020; Celik et al., 2020; Edtbauer et al., 2020; Eger et al., 2019; Friedrich et al., 2021;  
177 Pfannerstill et al., 2019; Tadic et al., 2020; Wang et al., 2020).

### 178 **2.2 Aerosol and Trace Gas Measurements**

179 Aerosol size distributions were measured using an Optical Particle Spectrometer (OPC, Grimm  
180 model 1.109) and a Fast Mobility Particle Spectrometer (FMPS, TSI model 3091). The OPC

181 measures particles in the size range 0.25 – 32  $\mu\text{m}$ , and the FMPS measures particles with sizes  
182 between 5.6 nm and 560 nm with 6s and 1s time resolution, respectively. The inlet for the aerosol  
183 instrumentation was located at the top of a measurement container at a horizontal distance of about  
184 15 m from the INP filter sampling unit (Figs. S3-S4). To avoid condensation in inlet lines, aerosol  
185 samples were passed through a drying system, which reduced ambient relative humidity (RH) to  
186 an average value of  $\approx 40\%$  in the measurement container. Ambient RH ranged between 67 and  
187 81% during INP sampling periods. OPC and FMPS data were averaged over 1-minute time  
188 intervals. A filter flag based on aerosol measurements was derived to identify and eliminate stack  
189 emissions and applied to all aerosol data. The filter flag was based on short term variation in  
190 particle number concentration measured by a Condensation Particle Counter (CPC, TSI model  
191 3787), black carbon concentrations (Aethalometer, Magee AE33), wind direction and speed. The  
192 flag was set when the apparent wind direction was from the direction of the stack ( $\pm 30^\circ$ ) as seen  
193 from the aerosol inlet position (Fig. S3) and strong fluctuations of black carbon and/or particle  
194 number concentrations were observed relative to background levels. Particle losses were estimated  
195 using the Particle Loss Calculator (von der Weiden et al., 2009). Losses were negligible ( $<1\%$ ) up  
196 to 3.5  $\mu\text{m}$  and increased to 40% at 10  $\mu\text{m}$ .

197 Particle surface area concentrations were derived from the 1-min time-averaged FMPS and OPC  
198 measurements as follows. Geometric diameters were estimated from the measured mobility  
199 diameters (FMPS) and optical particle diameters (OPC). Aerosols were assumed dry at sampling  
200 conditions following the drying system described above. To convert optical particle diameters into  
201 geometric diameters, it was assumed that all coarse particles ( $d_p > 3000\text{ nm}$ ) were composed of  
202 sea salt and dust with a mass ratio of 25% to 75%, and using the respective refractive indices and  
203 shapes the measured optical particle diameters were converted into geometric diameters (Sect.  
204 S1.1). The sea salt:dust mass ratio was based on average dust and sea salt concentrations as  
205 measured in particles  $< 10\ \mu\text{m}$  ( $\text{PM}_{10}$ ; see Sect. S2 for details).

206 Fine particle ( $d_p < 700\text{ nm}$ ) size was converted from optical diameter ( $d_{\text{opt}}$ ) into geometric diameter  
207 ( $d_{\text{geo}}$ ) using the optical properties calculated from the chemical composition of particles  $< 1\ \mu\text{m}$   
208 ( $\text{PM}_1$ ) as measured by an Aerosol Mass Spectrometer (Aerodyne HR-ToF-AMS), assuming  
209 spherical particles. For particles in the intermediate size range (700 – 3000 nm), log-linear  
210 interpolation of optical and spherical properties was applied for conversion of optical into

211 geometric particle diameters (Sect. S1.2). The mobility diameters measured by the FMPS were  
212 considered equivalent to the geometric diameter, assuming spherical particles. From the resulting  
213 particle size distributions, particle surface area was calculated for each size bin. Total particle  
214 surface concentrations were determined by integrating the surface area distribution for particles up  
215 to 10  $\mu\text{m}$  ( $d_{\text{geo}}$ ). The overall uncertainty of derived particle surface area concentrations is estimated  
216 to be 30%, including the uncertainty due to particle losses (see Sect. S3).

217 The water-soluble fraction of total suspended particles (TSPs) was monitored with hourly  
218 resolution using a Monitor for AeRosols and Gases in Ambient Air, MARGA (Metrohm Applikon  
219 model S2, Herisau, Switzerland). Sea salt concentrations were estimated by scaling measured  
220 soluble  $\text{Na}^+$  concentrations by 3.27 following Manders et al. (2009) and were used as a proxy for  
221 SSA number concentrations. Size-resolved single particle chemical composition measurements  
222 have shown that sea salt represents 50-70% of SSA particles by number ( $d_p > 0.5\mu\text{m}$ ) (Collins et  
223 al., 2014). Hourly composition data was linearly interpolated for 4 samples where 1-3 hours (of 7-  
224 24 hours total sampling time) was missing (Fig. S5). The MARGA sampling line was  
225 equipped with a  $\text{PM}_{10}$  cyclone, but the sample was not dried as the instrument is not prone to  
226 condensation. Particle transmission losses to the MARGA were estimated using the PLC and found  
227 to be consistent with the aerosol sizing instruments described above.

228 Nitric oxide (NO) concentrations were measured using a commercially available two-channel  
229 chemiluminescence monitor, CLD 790 SR (ECO Physics AG, Dürnten, Switzerland). During the  
230 AQABA campaign, the CLD 790 SR, MARGA, FMPS, OPC, HR-ToF-AMS, CPC and  
231 Aethalometer were operated within laboratory containers on the main deck of the research vessel.  
232 The NO measurements were used to prevent stack sampling during INP collection (see Sect. 2.4).

### 233 **2.3 Dust Mass Concentrations from MERRA-2**

234 Since dust concentrations were not measured during the campaign, hourly dust surface mass  
235 concentrations along the cruise track were obtained from the ( $0.5 \times 0.625^\circ$ ) Modern-Era  
236 Retrospective analysis for Research and Application, version 2 (MERRA-2; Gelaro et al., 2017)  
237 and were averaged over the region covered during each sampling period. Buchard et al. (2017)  
238 showed a high degree of correlation between MERRA-2 and surface dust concentration  
239 observations ( $r \geq 0.69$ ), particularly during dust storms ( $r \geq 0.92$ ). MERRA-2 surface dust mass



240 concentrations also correlated well with  $PM_{10}$  observed during AQABA ( $r \geq 0.71$ ) (Fig. S6).  
241 MERRA-2 uses the GEOS-5 Earth system model (Molod et al., 2015; Rienecker et al., 2011) with  
242 72 vertical layers between the surface and 0.01 hPa ( $\sim 80$  km) and the three-dimensional variational  
243 data assimilation Gridpoint Statistical Interpolation analysis system (Kleist et al., 2009; Wu et al.,  
244 2002, additional details in Sect. S4).

## 245 **2.4 INP Measurements in Aerosol**

246 Ambient aerosol sampling for offline measurement of INPs was conducted from 5 Jul – 31 Aug  
247 2017 on the *Kommandor Iona's* wheelhouse top (platform above the bridge),  $\sim 15$  m horizontally  
248 from the online aerosol measurements inlet and  $\sim 15$  m from the ocean surface (Figs. S3-4).  
249 Sampling locations along the cruise transect corresponding to each aerosol sample are shown in  
250 Figs. S1-2.

251 Aerosol samples were collected over 3-28 hour periods on polycarbonate filters (47 mm diameter,  
252  $0.2 \mu\text{m}$  pore-size, Whatman® Nuclepore, Chicago, Illinois, USA) placed in open-face Nalgene®  
253 Analytical Filter Units (Waltham, Massachusetts, USA). Sampling intervals and frequency were  
254 chosen with the aim of collecting  $> 5000$  L during dust events and  $> 10,000$  L when OPC particle  
255 counts were relatively low (e.g., during sampling periods f040-44), as conditions allowed. Aerosol  
256 sampling flow rates through the filter units were set to 10-13 LPM using a MassStream™ mass  
257 flow controller (Bethlehem, PA, USA) connected inline with a rotary vane pump (Thomas QR-  
258 0100, Gardner Denver ©, Monroe, LA, USA). To decrease exposure to stack emissions, the pump  
259 was automated to switch off when online measurements of NO exceeded one standard deviation  
260 above the average background concentration for over 1 minute ( $\sim 0.4 \pm 0.8$  ppb). Comparing the  
261 stack contamination filter flag for aerosol measurements (Sect. 2.2) with INP sampling periods  
262 additionally indicates no influence of stack emissions on INP filter samples. Lacking a size-  
263 selective inlet for INP sampling, it is possible that aerosols  $> 10 \mu\text{m}$  were present in INP samples  
264 during dust events. Surface area may be underestimated for these samples due to the  $PM_{10}$  cutoff  
265 for aerosol sizing (Sect. 2.2 and S3), but we do not expect this to affect our overall conclusions as  
266 increased aerosol surface area would further reduce  $n_s$  (see Results Sect. 3.3 and Discussion Sect.  
267 4). Prior to sampling, filters were cleaned by soaking in 10 % peroxide ( $H_2O_2$ ) for 10 minutes  
268 followed by rinsing three times with deionized water, the last rinse further “polished” by passage

269 through a 0.1  $\mu\text{m}$  pore-size syringe filter (Puradisc, Whatman  $\text{\textcircled{R}}$ , Maidstone, U.K). Filters were  
270 pre-loaded into filter units in a laminar flow hood to further minimize contamination from  
271 handling. After collection, each aerosol filter was placed in a 60 mm diameter sterile Petri dish  
272 (Life Science Products, Frederick, Colorado, USA) using pre-cleaned acetyl plastic forceps (Fine  
273 Science Tools, Foster City, California, USA), sealed with Parafilm and stored frozen ( $-20\text{ }^{\circ}\text{C}$ ).  
274 Samples were shipped in a dry shipper via Cryoport $\text{\textcircled{R}}$  High Vol Shipper at  $-180\text{ }^{\circ}\text{C}$  and upon  
275 arrival at the laboratory were stored at  $-80\text{ }^{\circ}\text{C}$  until processed, within 18 to 38 months since  
276 collection. To release collected particles, filters were immersed in 5-8 mL ultrapure water (Cat.  
277 Number W4502, Sigma-Aldrich $\text{\textcircled{R}}$ , St. Louis, MO, USA) and shaken by hand for 20 minutes just  
278 prior to measurement.

279 INP concentrations were measured using the Scripps Institution of Oceanography Automated Ice  
280 Spectrometer (SIO-AIS), an immersion freezing droplet assay instrument that is described in detail  
281 in Beall et al. (2017). Briefly, the aerosol sample suspensions and SSW samples were distributed  
282 in  $30 \times 50\text{-}\mu\text{L}$  aliquots into clean 96-well polypropylene sample trays (OPTIMUM $\text{\textcircled{R}}$  ULTRA  
283 Brand, Life Science Products). An equal number and volume of aliquots of ultrapure water  
284 accompanied each sample in the tray as a control. Trays were then inserted into an aluminum block  
285 that was cooled at  $-0.87\text{ }^{\circ}\text{C min}^{-1}$  until the samples froze. Cumulative INP number concentrations  
286 per temperature per volume liquid are calculated using the fraction ( $f$ ) of unfrozen wells per given  
287 temperature interval:

$$288$$
$$289 \quad n_{\text{INP,L}} = \frac{-\ln(f)}{V_d} \quad \text{Eq. (1)}$$

290

291 where  $V_d$  is the volume of the sample in each well (Vali, 1971). For aerosol filter samples,  
292 cumulative INP number concentrations are calculated using the ratio of the ultrapure water volume  
293 used for resuspension of the particles ( $V_{re}$ ) to the volume of air sampled ( $V_A$ ):

$$294$$
$$295 \quad n_{\text{INP}} = \frac{-\ln(f) \cdot V_{re}}{V_d \cdot V_A} \quad \text{Eq. (2)}$$

296

297 Prior to calculating  $n_{\text{INP}}$ , the fraction of unfrozen wells ( $f$ ) was adjusted for contamination in the  
 298 water used for suspension by subtracting the number of frozen ultrapure water wells per  
 299 temperature interval from both the total number of unfrozen wells and total wells of the sample.  
 300 The  $n_{\text{INP}}$  was additionally adjusted for background INPs from filters and sampling handling  
 301 processes. Background  $n_{\text{INP}}$  were estimated using measured  $n_{\text{INP}}$  in aerosol sample field blanks,  
 302 which had been placed in the sampling apparatus  $\sim 5$ s (without actuating the pump) before removal  
 303 and unloading and storage of the filter. Seven field blank samples were collected, one every  $\sim 7$   
 304 days of the cruise (Fig. S7). INP concentrations were measured in field blanks as described above,  
 305 and the  $n_{\text{INP}}$  simulated using the mean air volume sampled (6680 L). Figure S7 shows the  
 306 estimated  $n_{\text{INP}}$  across the 7 field blanks, which ranged between  $1.0 \times 10^{-4}$  and  $7.0 \times 10^{-3} \text{ L}^{-1}$  at  $-20$   
 307  $^{\circ}\text{C}$ . The freezing onset temperatures detected in the field blanks ranged between  $-6$  and  $-27$   $^{\circ}\text{C}$ . To  
 308 correct  $n_{\text{INP}}$  measured in aerosol samples for background INPs from sample handling, a linear  
 309 regression based on the geometric mean  $n_{\text{INP}}$  measured in field blank suspensions ( $\text{mL}^{-1}$  water)  
 310 was used to estimate background concentrations of INPs in samples at all temperatures between -  
 311  $14.5$   $^{\circ}\text{C}$  and  $-27$   $^{\circ}\text{C}$ . The estimated background  $n_{\text{INP}}$  was then subtracted from the INP  
 312 concentration measured in filter sample suspension volumes in this temperature range prior to  
 313 calculating  $n_{\text{INP}}$ . The  $n_{\text{INP}}$  measured in one aerosol sample (f033) fell within the estimated INP  
 314 background levels.

315 For this study, the detection limit was  $0.68 n_{\text{INP}} \text{ mL}^{-1}$  liquid or  $0.001\text{-}0.0024 n_{\text{INP}} \text{ L}^{-1}$  air for the  
 316 minimum and maximum air volume sampled, respectively. To extend the upper limit of detection  
 317 (i.e., the point at which all droplets have frozen) dilutions of 1:10 and 1:100 were performed on 8  
 318 samples (Fig. S8).

319 The ice-active surface site density,  $n_s$ , is a metric used to define the ice-nucleating capabilities of  
 320 an aerosol species (i.e., an aerosol sample of all the same particle type) (Kanji et al., 2017) as  
 321 follows:

$$322 \quad n_s = \frac{N_{\text{ice}}}{N_{\text{tot}} \times A \text{ (cm}^2\text{)}} \quad \text{Eq. (3)}$$

323 where  $N_{\text{ice}}$  is the number of frozen droplets,  $N_{\text{tot}}$  is the total number of particles in a monodisperse  
 324 aerosol population, and  $A$  is the surface area per particle.

325 The value of  $n_s$  can also be approximated for polydisperse aerosol samples containing multiple  
326 aerosol types:

$$327 \quad n_s = \frac{N_{ice}}{A_{tot} (cm^2)} \quad \text{Eq. (4)}$$

328 where  $A_{tot}$  is the total surface area of the polydisperse aerosol. The difference between the  $n_s$   
329 approximation (Eq. 4) and  $n_s$  (Eq. 3) is that many particle types are typically included in the  $n_s$   
330 approximation, and in an ambient aerosol measurement most of these are not IN-active (see also  
331 Hiranuma et al., (2015) Sect. 2.4). Furthermore, the subset of INPs in the sample are likely also of  
332 different types, which likely have different  $n_s$  in the strict sense (Eq. 3). Nevertheless, the  $n_s$   
333 approximation is a useful metric for comparing the ice-nucleating ability of different air masses  
334 and source regions and is often used for comparing data across studies of INPs measured in  
335 ambient air. It is extremely challenging to separate measurements of INPs and surface area by each  
336 particle type, and requires, for example, combining online measurements of single particle  
337 chemistry, size distributions and INPs (Cornwell et al., 2019). All  $n_{INP}$  and  $n_s$  are reported  
338 normalized to a standard temperature of 273.15 K and pressure of 1013 hPa.

339 Heat and peroxide treatments were applied to a subset of samples (12 of 26) to test for heat-labile  
340 biological (e.g., proteinaceous) and organic INP composition, respectively, following the  
341 procedure described in McCluskey et al. (2018b) and Suski et al. (2018). The 12 samples were  
342 selected based on sampling location with the aim of getting a representative measurement from  
343 each region. For each heat-treated sample, a 2 mL aliquot of the original ultrapure water suspension  
344 was heated to 95 °C for 20 min in a water bath and re-tested for changes in  $n_{INP}$ . For peroxide  
345 treatments, 1.6 mL of the original suspension was combined with 0.8 mL of 30% peroxide (Sigma  
346 Aldrich®, St. Louis, Missouri, USA) to achieve a final concentration of 10%, then the mixture  
347 was heated to 95 °C for 20 min while being illuminated with two 26-W UVB fluorescent bulbs.  
348 To remove residual peroxide and prevent freezing point depression, the solution was cooled and  
349 catalase (Cat. Number IC10042910, MP Biomedicals, Santa Ana, California, USA) was added  
350 Figure S7 shows the estimated  $n_{INP}$  in a heat and peroxide-treated blank sample. Fisher's Exact  
351 Test was applied to frozen and unfrozen well fractions between each untreated sample and its  
352 corresponding treated sample to test for significant differences ( $p < 0.05$ ). Note that significant  
353 difference in frozen well fraction is insufficient as a sole indicator of sensitivity in peroxide treated

354 samples because samples are diluted 2:3 (by 33%) compared to untreated samples. As  $n_{\text{INP}}$  can be  
355 corrected for the dilution by scaling (as opposed to frozen well fractions), the overlap in 95%  
356 binomial sampling confidence intervals (Agresti and Coull, 1998) between the untreated and  
357 peroxide-treated sample is an additional indicator of sensitivity for a given data point in the  
358 peroxide-treated sample spectrum within  $\pm 0.2$  °C, the uncertainty in the SIO-AIS temperature  
359 measurement (Beall et al., 2021). A lack of overlap in the 95% binomial sampling confidence  
360 interval within  $\pm 0.2$  °C equates to a significance threshold of  $p < 0.005$  (Krzywinski and Altman,  
361 2013).

362 INP concentrations were additionally measured in in untreated, heat-treated, and peroxide-treated  
363 subsamples from an archived suspension of the soil dust sample N12 SD for comparison with this  
364 study (DeMott et al., 2018; hereafter referred to as “N12-SD”). Briefly, the sample was generated  
365 during the recent laboratory intercomparison of INP measurements(, collected on a  $0.2 \mu\text{m}$   
366 Nuclepore polycarbonate membrane filter (Whatman ®, Chicago, Illinois, USA) and stored frozen  
367 at  $-20$  °C until processed, as described in DeMott et al (2018).

368

## 369 **2.5 INP Measurements in SSW**

370 INP concentrations were additionally measured in 10 SSW samples. For seawater sampling, a  
371 water intake vertical steel pipe was positioned on the starboard of the ship approximately 2 m  
372 below the sea surface level. The seawater was pumped into a 200 L stainless steel tank and  
373 continuously exchanged at a rate of  $3000 \text{ L h}^{-1}$ . SSW samples for INP analysis were collected in  
374 15 mL sterile centrifuge tubes (Falcon™, ThermoFisher Scientific, Waltham, Massachusetts,  
375 USA) and stored frozen at  $-20$  °C until they could be shipped in a dry shipper via Cryoport® ( $-180$   
376 °C) and ultimately stored at  $-80$  °C as for aerosol samples until processed as described above (Sect.  
377 2.4), within 18 to 38 months since collection. Storage duration was not correlated with INP  
378 concentration changes in frozen marine and coastal precipitation samples (Beall et al., 2020). Heat  
379 and peroxide treatments as described above were applied to 5 SSW samples from the Arabian Sea  
380 and the Gulf of Aden. The focus on these regions was motivated by the detection of marine aerosol  
381 originating from the upwelling region in Somalia reported in Edtbauer et al., (2020; see Sect.  
382 3.3). To assess the contribution of submicron INPs to total measured INPs, 2 mL of SSW was

383 filtered through a 0.2  $\mu\text{m}$  sterile syringe-filter (Acrodisc® Pall®, Port Washington, New York,  
384 USA) and re-tested.

385 INP concentrations in SSW collected at the Ellen Browning Scripps Memorial Pier at Scripps  
386 Institution of Oceanography (SIO; 32.8662 N, 117.2544 W) were assessed in 17 samples for  
387 comparison with SSW collected during AQABA. Samples were collected between 31 Jan and 7  
388 May 2016 in 15-30 mL sterile centrifuge tubes (Falcon™, ThermoFisher Scientific, Waltham,  
389 Massachusetts, USA) at depths of 1-3m and processed immediately using the SIO-AIS as  
390 described above.

### 391 **3 Results**

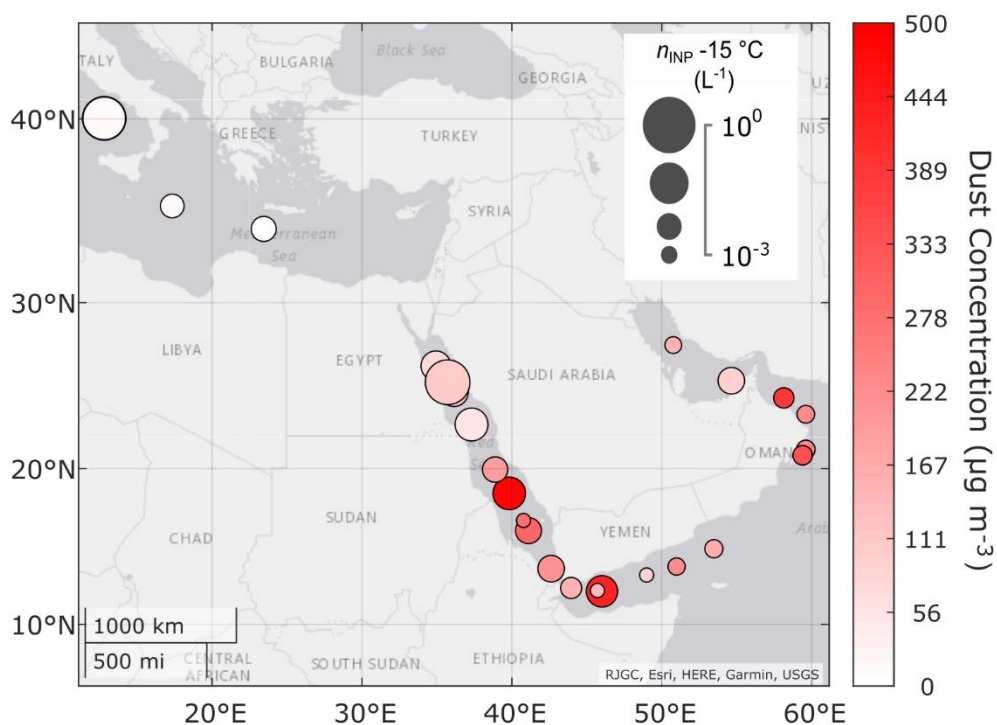
#### 392 **3.1 INP Concentrations in Aerosol**

393 A total of 26 aerosol samples were collected in July – August 2017 during AQABA for offline  
394 measurements of INPs. The INP concentrations ( $n_{\text{INP}}$ ) measured in samples collected in the  
395 Mediterranean Sea, the Red Sea, the Gulf of Aden, Arabian Sea, Gulf of Oman, and Arabian Gulf  
396 spanned up to 2 orders of magnitude at -15 °C (Fig. 1, Table 1), between  $5 \times 10^{-3}$  and  $5 \times 10^{-1} \text{ L}^{-1}$   
397 <sup>1</sup>. This range agrees within an order of magnitude with that of Prodi et al. (1983) who measured  
398  $n_{\text{INP}}$  in the Mediterranean, Red Sea, Gulf of Aden and Indian Ocean nearly 4 decades prior to the  
399 present study ( $4 \times 10^{-2}$  to  $2 \text{ L}^{-1}$  at -16 °C). Average ambient dust concentrations during each  
400 sampling period ranged from 2-490  $\mu\text{g m}^{-3}$  (PM<sub>10</sub> Table 1). There is no agreed-upon standard for  
401 definition of extreme dust events in the literature, though the 24-hr average WHO or US EPA  
402 health standards for average PM<sub>10</sub> are commonly used (Gandham et al., 2020; Khaniabadi et al.,  
403 2017). Using the US EPA health standard for PM<sub>10</sub> as a threshold for extreme events ( $150 \mu\text{g m}^{-3}$ ,  
404 <sup>3</sup>), 14 of the 26 samples were collected during dust events. This is conservative given the equivalent  
405 WHO guideline for PM<sub>10</sub> is  $50 \mu\text{g m}^{-3}$  (WHO, 2005), in which case 22 of the 26 sampling periods  
406 would be classified as dust events. Prior studies have reported comparable PM<sub>10</sub> levels during dust  
407 events in the region (Gandham et al., 2020; Krasnov et al., 2016; Shahsavani et al., 2012).

408 Figs. S9-S10 show the extent of k-means clustered FLEXPART back-trajectories below the  
409 altitude of 1500 m (see Sect. S5 for details). This threshold was applied to eliminate most of the  
410 free tropospheric parts of the back-trajectories and was selected based on the MERRA-2 monthly

411 average planetary boundary layer (PBL) heights during the campaign period, which were 200-700  
 412 m over the ocean and up to 1700 m over land. FLEXPART air mass back trajectories show that  
 413 many samples collected during extreme dust events (f013, f014, f016, f018, and f020) were  
 414 influenced by emissions from North Africa and the Arabian Peninsula (Figs S8-S9). Other source  
 415 regions included the Mediterranean, Nile Delta, Sinai Peninsula (f006-f008, f038), Northeast  
 416 Egypt (f009-f010), Iran (f023-f024), and Southern and Eastern Europe (f040, f042, f044). The  
 417 ranges of aerosol surface area concentrations for all sampling periods were  $< 320 \mu\text{m}^2 \text{cm}^{-3}$ , with  
 418 the exception of f024, for which aerosol surface area range was  $> 600 \mu\text{m}^2 \text{cm}^{-3}$  (Table 1).

419



420

421 **Figure 1.** Map of the sample locations for 26 aerosol samples collected on the RV *Kommandor*  
 422 *Iona* during Air Quality and climate change in the Arabian Basin (AQABA; see also Figs. S1-S2  
 423 and S9-S10). Measured  $n_{\text{INP}}$  spanned 2 orders of magnitude at  $-15 \text{ }^\circ\text{C}$ , from  $5 \times 10^{-3}$  to  $5 \times 10^{-1} \text{ L}^{-1}$   
 424 <sup>1</sup>. Marker sizes indicate abundance of INPs. Marker colors indicate the average ambient dust mass  
 425 concentration during the sampling period from hourly MERRA-2 reanalysis data.

427 **Table 1.** Summary of aerosol samples collected during AQABA. “—” indicates where data are  
 428 missing; “NaN” indicates values below detection limit. Locations are given at the transect  
 429 midpoint during each sampling period.

Sample ID	Start datetime (UTC)	Stop datetime (UTC)	Latitude (° N)	Longitude (° E)	$n_{\text{INP}}^{-15\text{ °C}}$ (L <sup>-1</sup> )	Sample Volume (L air)	Average Aerosol Surface Area (PM <sub>10</sub> , μm <sup>2</sup> cm <sup>-3</sup> )	Aerosol Surface Area [min, max] (PM <sub>10</sub> , μm <sup>2</sup> cm <sup>-3</sup> )	Average Dust Concentration (PM <sub>10</sub> , μg m <sup>-3</sup> )	Average Seasalt Concentration (PM <sub>10</sub> , μg m <sup>-3</sup> )
f006	05-Jul 05:46	05-Jul 11:37	26.224	35.025	0.0146	3370	290	[199, 375]	170	-
f007	05-Jul 16:40	05-Jul 19:51	26.291	34.933	0.0475	2588	260	[222, 289]	70	-
f008	06-Jul 07:09	06-Jul 14:08	25.225	35.775	0.1161	5225	177	[106, 259]	100	-
f009	07-Jul 05:50	07-Jul 15:07	25.011	35.947	0.0838	6940	352	[253,416]	110	-
f010	08-Jul 16:33	09-Jul 05:59	23.623	36.931	0.0592	8073	219	[163, 287]	50	-
f013	14-Jul 12:26	14-Jul 16:13	18.687	39.672	0.0585	2283	264	[176, 352]	490	10
f014	15-Jul 05:10	15-Jul 11:49	16.552	40.834	0.0348	4000	271	[204, 343]	300	5
f016	18-Jul 07:04	18-Jul 14:52	11.939	45.334	0.0534	4690	265	[158, 391]	430	-
f018	22-Jul 10:20	22-Jul 18:44	20.941	59.474	0.0166	5025	212	[171, 238]	340	-
f019	23-Jul 04:48	23-Jul 13:34	21.410	59.691	0.0145	5270	218	[190, 240]	240	-
f020	25-Jul 17:15	26-Jul 04:02	23.976	58.809	0.0184	6511	-	-	390	5
f023	04-Aug 04:05	04-Aug 11:56	28.084	50.284	0.0112	4720	835	[756, 965]	150	4
f024	05-Aug 05:57	05-Aug 13:53	25.432	53.853	0.0371	5221	357	[206, 827]	90	-
f025	07-Aug 09:26	07-Aug 16:46	23.814	59.186	0.0129	4410	55	[46, 72]	220	12
f030	13-Aug 07:08	14-Aug 11:06	15.970	54.705	0.0132	15111	28	[16, 144]	160	-
f031	14-Aug 15:03	15-Aug 09:03	14.003	52.357	0.0121	12972	25	[19, 105]	230	-
f032	15-Aug 09:42	15-Aug 15:07	13.354	49.432	0.0059	3260	96	[82, 147]	80	6
f033	16-Aug 09:30	16-Aug 13:17	12.208	45.706	NaN	2280	73	[51, 135]	130	2
f034	16-Aug 13:27	17-Aug 07:04	12.177	45.429	0.0206	8464	168	[51, 372]	150	1
f035	17-Aug 07:30	17-Aug 14:55	13.308	42.974	0.0365	4460	340	[244, 409]	210	2
f036	18-Aug 06:36	18-Aug 15:03	16.290	41.038	0.0057	6634	208	[160, 428]	280	2
f037	19-Aug 07:05	20-Aug 07:04	18.699	39.609	0.0326	18806	240	[175, 331]	190	7
f038	21-Aug 07:22	21-Aug 16:01	24.112	36.554	0.0422	6700	256	[202, 295]	150	-
f040	26-Aug 16:02	27-Aug 07:04	33.803	24.814	0.0314	9030	90	[58, 142]	< 10	3
f042	28-Aug 07:51	28-Aug 16:02	35.310	17.965	0.0279	6396	163	[131, 222]	< 10	2



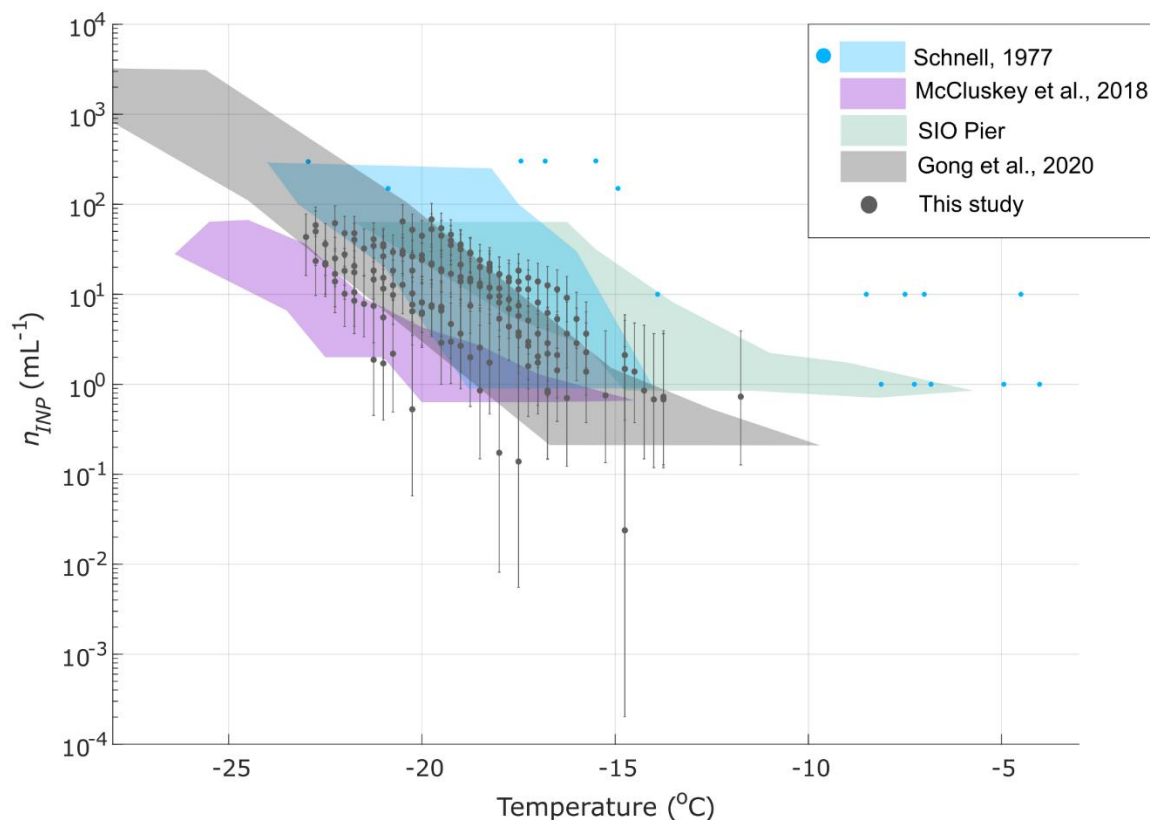
### 430 3.2 Seawater Source Potential

431 The  $n_{\text{INP}}$  values in 10 SSW samples collected during AQABA were used to characterize the INP  
432 source potential of SSA generated by bubble bursting (Wang et al., 2017). Results from prior  
433 studies have demonstrated that jet droplets are a more efficient transfer vehicle than film drops of  
434 INPs into SSA particles (Mitts et al., 2021; Wang et al., 2017). We measured the  $n_{\text{INP}}$  in SSW to  
435 test whether the seawater source strength was comparable to that of prior studies, or whether the  
436 SSW was possibly enriched with INPs due to biological activity or even dust deposition (Cornwell  
437 et al., 2020).

438 Figure S11 shows how the  $n_{\text{INP}}$  measured at  $-19\text{ }^{\circ}\text{C}$  in 10 seawater samples varied by the sample  
439 collection location. Concentrations ranged between 1 and  $50\text{ }n_{\text{INP}}\text{ mL}^{-1}$  and were highest between  
440 the Gulf of Oman and the Gulf of Aden. This region exhibited relatively high chlorophyll  $a$  during  
441 the cruise, with levels between 1 and  $30\text{ mg m}^{-3}$  (Fig. S12). In Fig. 2,  $n_{\text{INP}}$  were compared with  
442 SSW from the Ellen Browning Scripps Memorial Pier in coastal Southern California (SIO Pier),  
443 Cabo Verde in the Northeast Atlantic, the Southern Ocean (McCluskey et al., 2017), and the  
444 Northwest Atlantic (Schnell, 1977). AQABA  $n_{\text{INP}}$  were most comparable with Gong et al.'s  
445 (2020) observations in Cabo Verde. The lack of any unusually high INP spectra suggests that INP  
446 enrichment due to dust deposition (Cornwell et al. 2020) was absent or infrequent. It is possible  
447 that storage of SSW samples (Sect. 2.5) could have decreased measured  $n_{\text{INP}}$ , though we expect

448 that  $n_{\text{INP}}$  would be decreased by no more than  $10\times$  in untreated samples stored frozen (see  
449 discussion below).

450



451

452 **Figure 2.** Measured  $n_{\text{INP}}$  in 10 SSW samples collected during AQABA. Also shown are the  
453 composite INP spectrum of 14 coastal SSW samples collected on São Vicente Island, Cabo Verde  
454 (Gong et al., 2020), 17 coastal SSW samples collected at the Ellen Browning Scripps Pier (green  
455 shading), and 12 SSW samples collected in the Southern Ocean (McCluskey et al., 2018d).  
456 Schnell's (1977) SSW measurements are represented as a composite spectrum of 24 samples (blue  
457 shaded region) and 5 additional spectra (blue markers) from samples that exhibited higher freezing  
458 temperatures. All spectra presented are uncorrected for freezing point depression.

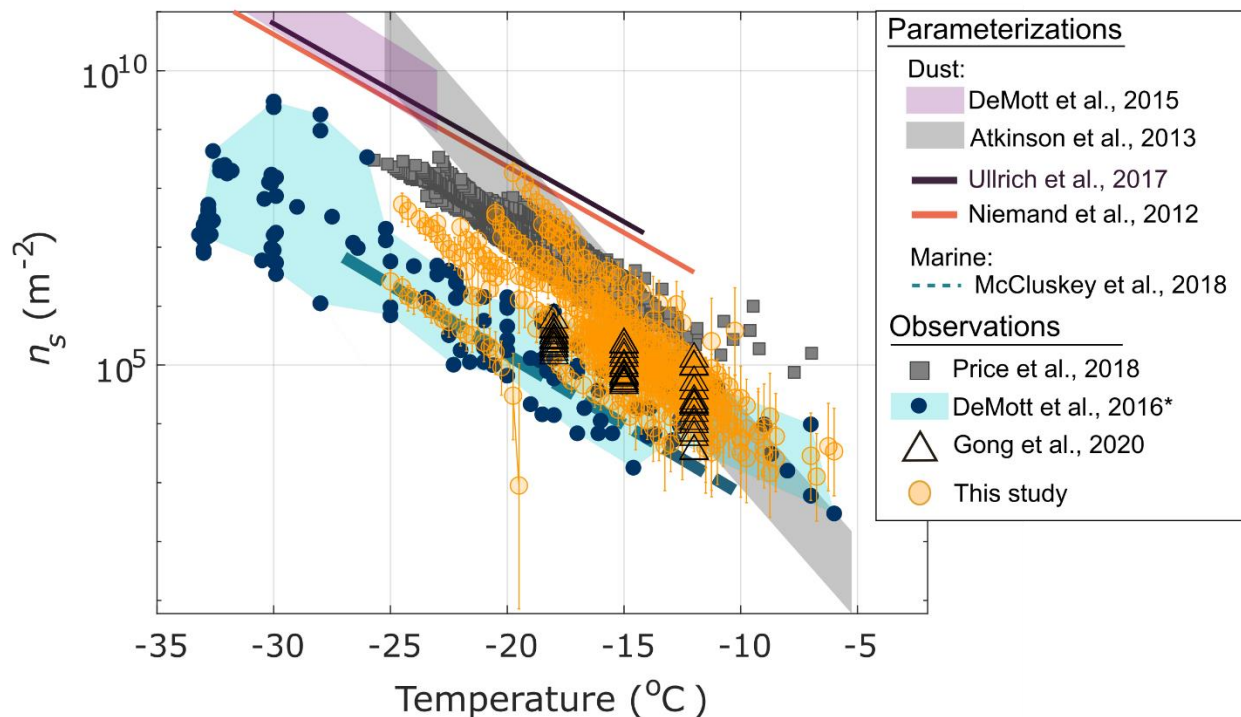
459 Offline treatments for testing heat lability, organic composition, and size were applied to 5 of the  
460 10 seawater samples (Methods Sec. 2.5). Heat and  $0.2\ \mu\text{m}$  filtering treatments suggest that a large  
461 fraction of the seawater INPs were heat sensitive and larger than  $0.2\ \mu\text{m}$  (Fig. S13). These results

462 are indicative of the POC type of marine INP defined in McCluskey et al. (2018a), though this  
463 result should be interpreted with caution as storage could potentially have increased sensitivity to  
464 filtering treatments.

465 Understanding of storage impacts on INPs measured in SSW is lacking. However, Beall et al.,  
466 (2020) showed that average INP concentration changes for untreated coastal precipitation samples  
467 due to frozen storage were within  $2\times$  of  $n_{\text{INP}}$  measured in fresh samples, with changes at the upper  
468 or lower end of the 95% CI exceeding  $10\times$  for some freezing temperatures. If SSW samples are  
469 similarly sensitive to storage, we would expect INP concentration changes to be within  $2\times$  on  
470 average, but up to  $> 10\times$  for any particular untreated sample. Beall et al. (2020) also reported  
471 similar changes INPs  $< 0.45 \mu\text{m}$  with a greater tendency toward losses, which indicates that storage  
472 may have caused increased sensitivity to the filter treatments applied to stored samples.

### 473 **3.3 Ice-active Surface Site Densities in Aerosol**

474 In Fig. 3, approximated ice-active surface site densities ( $n_s$ ) in aerosol samples are compared with  
475 multiple population-specific observations and parameterizations for dust and marine INPs. The  
476 AQABA measurements are also compared with observations from dust-laden air over the Tropical  
477 Atlantic (Price et al., 2018). Overall, observations nearly bridge the full regime between the M18  
478 parameterization for marine INPs (McCluskey et al., 2018c), and multiple dust INP  
479 parameterizations based on laboratory studies of surface dust. At higher temperatures, between -5  
480 and -12 °C, most observations show agreement with the composite spectrum of  $n_s$  observed in a  
481 range of marine and coastal environments from DeMott et al. (2016) and Yang et al. (2020), and/or  
482 the A13 K-feldspar parameterization. Between -10 and -20 °C, several samples agree with the M18  
483 marine INP parameterization within an order of magnitude, whereas two to three  $n_s$  spectra  
484 approach the U17 and N12 laboratory-derived dust INP parameterizations within an order of  
485 magnitude (Niemand et al., 2012; Ullrich et al., 2017), depending on temperature. Multiple  
486 samples (~8) additionally agreed with Price et al.'s (2018) observations of INPs between 30-3500  
487 m above the dust-laden Tropical Atlantic, and most agree with the Gong et al. (2020) surface-level  
488 observations, measured at Cabo Verde in the same region as Price et al. (2018).



490

491 **Figure 3.** Ice-active surface site densities ( $n_s$ ) as a function of temperature for 25 of 26 aerosol  
 492 samples collected during AQABA. Gong et al. (2020) and Price et al. (2018) measured INPs in  
 493 dust-dominant air masses in the tropical east Atlantic, with minor contributions from SSA, while  
 494 the DeMott et al. (2016) measurements were collected across a range of locations and conditions  
 495 within the marine boundary layer comprising air masses mostly dominated by relatively pristine  
 496 marine SSA. INP concentrations measured in sample f033 were below the detection limits imposed  
 497 by field blanks (see Sect. 2.4, Fig. S7). Error bars represent 95% binomial sampling confidence  
 498 intervals (Agresti and Coull, 1998). Sample f020 is not shown due to missing aerosol surface area  
 499 data during the sampling period. For the 8 samples on which a dilution was performed (Fig. S8),  
 500  $n_s$  for both the raw undiluted and diluted sample are shown. \*DeMott et al. (2016) data shown have  
 501 been updated with additional data from Yang et al. (2020).

502 Considering the frequency of dust events encountered (dust concentration  $> 150 \mu\text{g m}^{-3}$ , see Table  
 503 1), and the high probability that dust was the dominant aerosol source during most sampling  
 504 periods, it is striking that most  $n_s$  spectra observed are 1-3 orders of magnitude lower than the

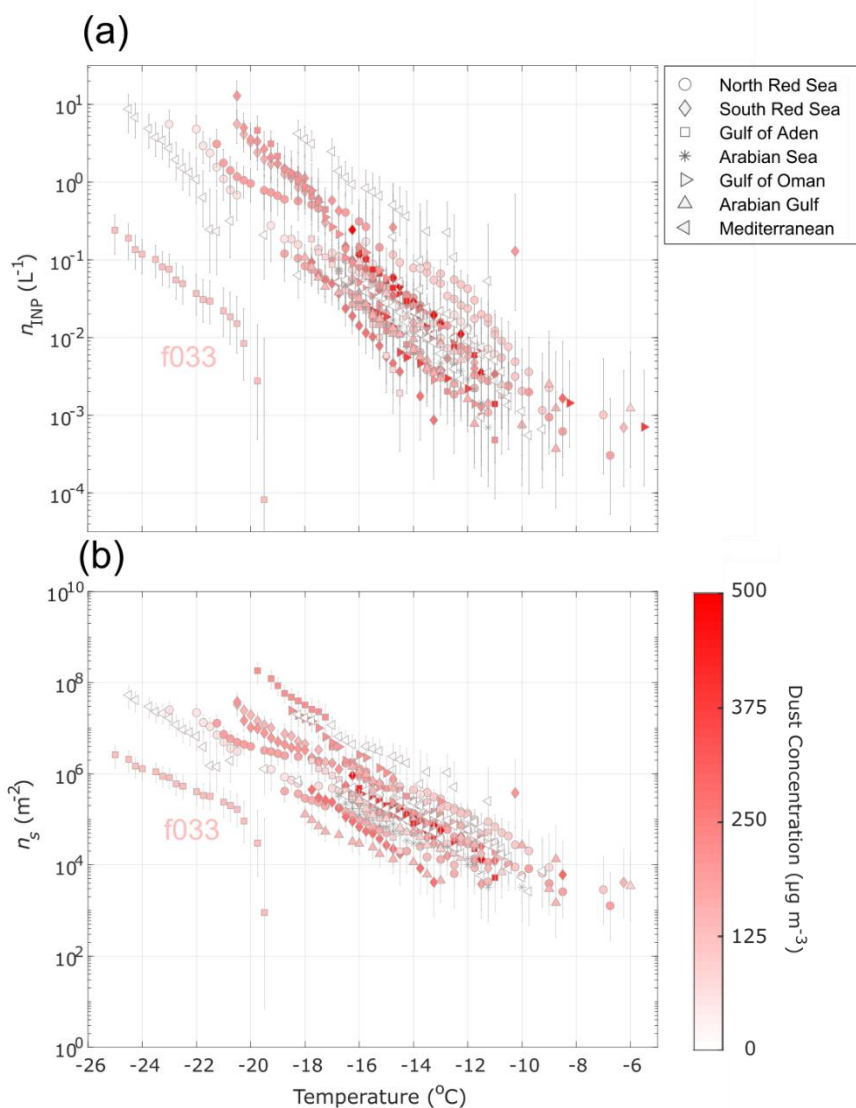
505 values predicted by dust parameterizations. As noted in Gong et al. (2020), some deviations could  
506 be expected due to the difference between approximated  $n_s$  based on total particle surface area in  
507 ambient measurements and true  $n_s$  based on surface area of a homogeneous aerosol population (see  
508 Methods Sect. 2.4)..

509 Given the marine environment in which sampling took place, a significant amount of sea spray  
510 aerosol (SSA) was also detected in many of the sampled airmasses, using sea salt as a proxy (Table  
511 1), and likely present in others for which no composition data were available. Edtbauer et al. (2020)  
512 reported the detection of high levels of dimethyl sulfide (DMS, up to 800 ppt) in the Gulf of Aden  
513 associated with a local phytoplankton bloom during AQABA (as evidenced by visible  
514 bioluminescence around the ship at night) as well as high levels of dimethyl sulfone (DMSO<sub>2</sub>) and  
515 other marine biogenic volatile organic carbons (VOCs) from the Somalian upwelling region. As  
516 mentioned above, the  $n_s$  for most samples between -6 and -18 °C agree with  $n_s$  derived from  
517 observations across various locations within the marine boundary layer (Fig. 3). However,  
518 considering that SSA is associated with 1000 times fewer IN sites per unit surface area than dust  
519 (i.e. 1000× lower  $n_s$ ) (McCluskey et al., 2018c), the characteristically low IN activity of untreated  
520 SSW (even in light of the modest changes expected from storage, Sect. 3.2), and the frequency of  
521 dust events during AQABA, our findings suggest it is unlikely that the observed INPs originated  
522 from SSA. . In general, detection of marine INPs in ambient aerosol is challenging due to their low  
523 relative abundance and decreased efficiency compared to dust (DeMott et al., 2016; McCluskey et  
524 al., 2018c). Thus, while SSA contributed to the measured aerosol surface area (Table 1), it is  
525 unlikely that the INPs observed in this study were marine in origin, or at least that this is  
526 indiscernible in the present study or based on present parameterizations of these populations.

527 Heterogeneous aerosol composition in the sampled air masses likely contributed to some of the  
528 low  $n_s$  spectra observed due to the contribution of non-INPs to the measured aerosol surface area  
529 (see description of  $n_s$  approximation in Sect. 2.4). However, the difference between  $n_s$  observed  
530 during the most extreme dust events, i.e., when the aerosol population was likely approaching  
531 homogeneity in composition, and the  $n_s$  predicted from N12 and U17 was still greater than 2 orders  
532 of magnitude. Figures 4(a) and (b) show overlap in  $n_{INP}$  and  $n_s$  observed in samples collected in  
533 low dust and high dust conditions, indicating that the INP populations observed during AQABA  
534 exhibited similar IN activity despite variation in total aerosol composition and dust loading. No

535 correlation was found between  $n_{\text{INP}}$  and aerosol surface area (Fig. S14),  $\text{PM}_{10}$  or dust concentration.  
536 This result is in contrast to Price et al. (2018) who found the variability in  $n_{\text{INP}}$  to be largely  
537 determined by variability in dust loading or aerosol surface area. Price et al. (2018) reported higher  
538 maximum aerosol surface area concentrations of  $\sim 1500 \mu\text{m cm}^{-3}$  from three samples collected in  
539 an exceptionally optically thick layer, compared to the maximum of  $965 \mu\text{m cm}^{-3}$  in the present  
540 study (Table 1). Yet overall, the aerosol surface area concentrations compare very well with those  
541 observed by (Price et al., 2018), indicative of comparable dustiness in the two studies. Excluding  
542 the case mentioned above, the average aerosol surface area was  $227 \pm 68 \mu\text{m}^2 \text{cm}^{-3}$  vs.  $226 \pm 26$   
543  $\mu\text{m}^2 \text{cm}^{-3}$  for the present study. Furthermore, the sample with the highest  $n_s$  at  $-15 \text{ }^\circ\text{C}$  (f044) was  
544 collected when dust concentrations were lowest ( $< 10 \mu\text{g m}^{-3}$ ) (Fig. 4, Table 1). This is also in

545 direct contrast to Price et al. (2018), who found that the highest  $n_s$  observed corresponded to the  
 546 highest dust loading.



547  
 548 **Figure 4.** INP concentrations ( $n_{\text{INP}}$ ) **(a)** and ice-active surface site densities ( $n_s$ ) **(b)** as a function  
 549 of temperature for 26 aerosol samples collected during AQABA. Markers are colored by the  
 550 average ambient dust concentration for the respective sampling period. Error bars represent 95%  
 551 binomial sampling confidence intervals (Agresti and Coull, 1998). The  $n_s$  measured in samples  
 552 collected during low dust conditions are equal to or greater than (up to 100×) the  $n_s$  measured  
 553 during dust events between -9 and -18 °C. INP concentrations measured in sample f033 were  
 554 below the detection limits imposed by field blanks (see Sect. 2.4, Fig. S7). Sample f020 is not

555 shown in (b) due to missing aerosol surface area data during the sampling period. For the 8 samples  
556 on which a dilution was performed (Fig. S8),  $n_s$  for both the raw undiluted and diluted sample are  
557 shown.

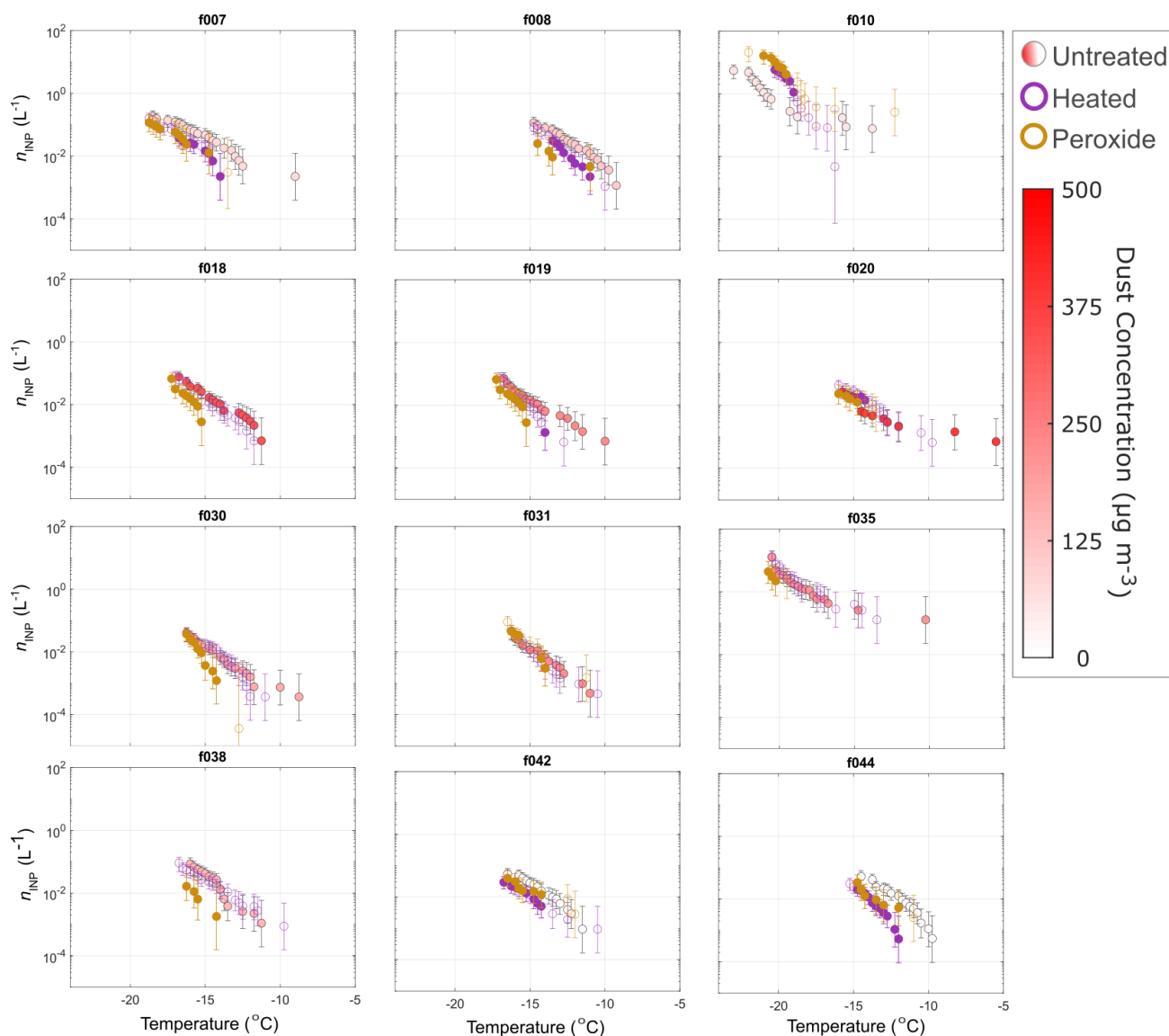
### 558 **3.4 Characterization of INPs in Aerosol**

559 Offline treatments for testing heat lability and organic composition of INPs were performed on 12  
560 samples via heat and peroxide treatments, respectively (Fig. 5). Prior studies have shown that the  
561 IN-active component of various types of mineral dusts are insensitive to heat treatments (Conen et  
562 al., 2011; Hara et al., 2016; Hill et al., 2016; O’Sullivan et al., 2014). The IN activity of K-feldspar,  
563 the dominant ice-nucleating component of mineral dust, was additionally found to be insensitive  
564 to digestion with peroxide (O’Sullivan et al., 2014). A small number of studies reported  
565 degradation of IN activity with peroxide treatment and/or heat treatment in Arizona Test Dust  
566 (ATD), that they attributed to organic material (Perkins et al., 2020; Yadav et al., 2019). Thus, we  
567 assume here that any degradation of IN activity due to heat and peroxide treatment correspond to  
568 loss of heat-labile (e.g. proteinaceous) and heat-stable organic INPs, respectively.

569 Fisher’s Exact Test was applied to frozen and unfrozen well fractions for each untreated sample  
570 and its corresponding treated sample to test for significant differences ( $p < 0.05$ ). Sensitivity to  
571 peroxide in most samples (i.e., INP degradation) demonstrate the consistent presence of stable  
572 organic INPs at temperatures  $\geq -15$  °C. The lack of peroxide sensitivity at temperatures  $< -15$  °C  
573 indicates dominance by mineral dust INPs at lower temperatures. Heat sensitivity in five samples  
574 suggests that biological INPs contributed to their warmest freezing INPs. Gong et al. (2020)  
575 similarly found heat-sensitivity in INPs at temperatures  $> -10$  °C. Four of the 12 samples exhibited  
576 heat sensitivity at relatively moderate temperatures  $-11$  to  $-18$  °C, including the two samples  
577 collected in the Mediterranean Sea. One sample (f010) exhibited increased  $n_{\text{INP}}$  in freezing  
578 temperatures  $< -18$  °C after heat and peroxide treatments. That the response to both heat and  
579 peroxide were nearly identical (Fig. 5) suggests that compounds may have been released from the  
580 surface during heating, uncovering a more IN active surface underneath (heating was common to  
581 both procedures). The increased  $n_{\text{INP}}$  post heat and peroxide treatment is an unexpected result given  
582 previous studies on treated soil dust measurements (Conen et al., 2011; Hill et al., 2016; O’Sullivan  
583 et al., 2014; Tobo et al., 2014). However, increases in IN activity after heat treatment have been



584 reported previously for airborne Saharan desert dust and aerosol collected during Saharan dust  
 585 intrusions (Boose et al., 2019; Conen et al., 2022) as well as SSA and precipitation (Martin et al.,  
 586 2019; McCluskey et al., 2018a) and should be further investigated in future studies. An increase  
 587 in IN activity after peroxide treatment has also been reported in a Himalayan dust sample  
 588 (Paramonov et al., 2018).



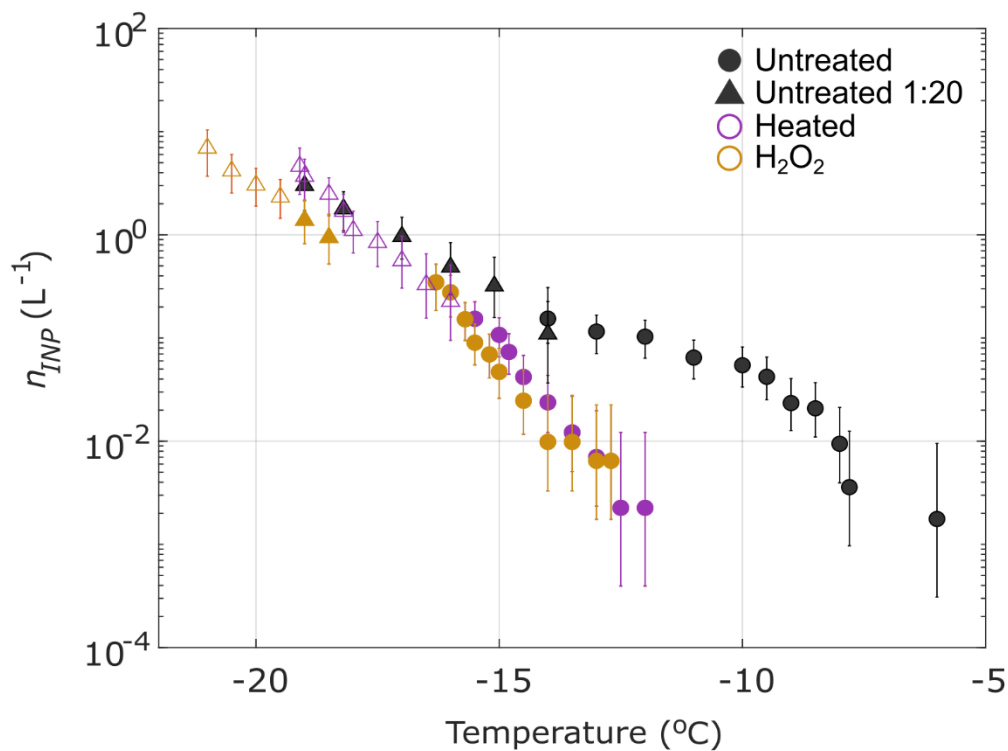
589 **Figure 5.** INPs in aerosol samples treated with heat and peroxide (Methods Sec. 2.4) to test for  
 590 INP heat-lability and organic composition. Markers of untreated spectra are colored by the average  
 591 dust concentration during the sampling period. Markers of heat-treated and peroxide-treated  
 592 samples are filled to indicate significant INP concentration difference from untreated samples  
 593

594 according to Fisher's Exact Test ( $p < 0.05$ ). Sensitivity to peroxide is evident for all samples  $\geq -$   
595 15 °C, indicative of stable organic INPs. Heat-lability is also evident at high to moderate  
596 temperatures in multiple samples, demonstrating that biological (e.g., proteinaceous) INPs also  
597 contributed to INPs observed during AQABA.

598 Given the frequency of dust events and generally high concentrations of dust during most sampling  
599 periods, it is surprising that most samples exhibit peroxide sensitivity. Aridisols and entisols are  
600 the dominant soil types in North Africa and the Arabian Peninsula (Nortcliff, 2012). Both types  
601 are associated with the lowest levels of organic carbon, commonly used as a proxy for total soil  
602 organic matter, compared to other soil types (3 and 9 g kg<sup>-1</sup>, respectively) (Yost and Hartemink,  
603 2019).

### 604 **3.5 Characterization of INPs in a Soil Dust Sample**

605 INP measurements of soil dusts in this region are scarce and have only been reported for a single  
606 surface dust soil sample, sample "SD", collected 50 km north of Cairo (Niemand et al., 2012).  
607 FLEXPART back-trajectories indicate this source region for several samples (f006-10, f038),  
608 though it should be noted that dust sources cannot be confirmed in this study lacking aerosol and  
609 soil dust mineralogy. For comparison with this study, we measured INPs in untreated, heat-treated,  
610 and peroxide-treated subsamples of an archived suspension of the N12-SD sample (Methods Sect.  
611 2.4; DeMott et al., 2018) . . Sample N12-SD exhibits sensitivity to both heat and peroxide at  
612 temperatures  $> -16$  °C, indicating biological composition of INPs at high freezing temperatures.  
613 Multiple AQABA samples influenced by desert air mass sources show similar sensitivities at  
614 higher temperatures: f006, f007, f019, and f020. Several others exhibit only peroxide-sensitivity  
615 in this temperature range. Overall, the heat and peroxide sensitivities in the N12-SD sample  
616 indicate that desert dusts may contribute biological and/or organic INPs at moderate to high-  
617 freezing temperatures, such as those observed in AQABA samples. Gong et al.'s (2020) results  
618 showing heat-sensitivity in INPs at temperatures  $> -10$  °C further demonstrate the contribution of  
619 biological INPs at high temperatures in dust-laden air masses near North Africa.



620  
 621 **Figure 6.** Measured concentrations of INPs in an aerosolized soil dust sample “N12-SD”, collected  
 622 50 km north of Cairo, Egypt (Niemand et al., 2012), that was treated with heat and peroxide to test  
 623 for INP heat-lability and organic composition, same as in Fig. 5 above (Methods Sec. 2.4). A 1:20  
 624 dilution of the sample is shown (triangles) and markers of heat-treated and peroxide-treated  
 625 samples are filled to indicate significant INP concentration differences from untreated samples  
 626 according to Fisher’s Exact Test ( $p < 0.05$ ). Sensitivity to peroxide and heat treatments indicates  
 627 biological INPs between -6 and -16 °C.

#### 628 4 Discussion

629 Considering the high freezing temperatures observed, evidence of organic composition, and  
 630 FLEXPART back trajectories showing that aerosol sources included populous regions and at least  
 631 one agriculturally active region (the Nile River Delta; Figs. S9-S10), it is possible that agricultural  
 632 soil dusts contributed to some of the relatively higher  $n_s$ ,  $n_{INP}$ , and heat and peroxide sensitivity  
 633 observed during AQABA. A range of  $n_s$  has been reported in studies of agricultural soil dusts, the  
 634 lower end of which agrees with the  $n_s$  observed in the present study between -8 and -25 °C (Fig.  
 635 3; Steinke et al., 2016; Tobo et al., 2014; O’Sullivan et al., 2014). Samples from air masses

636 influenced by the Nile River Delta or Southern Europe (f007-8, f010, f038, f042, f044) show a  
637 higher fraction of heat-sensitive INPs (Fig. 5). Heat-sensitivity is indicative of biological INPs,  
638 which have been associated with agricultural soil dusts in prior studies (Hill et al., 2016;  
639 O’Sullivan et al., 2014). Hill et al. (2016) and O’Sullivan et al. (2014) showed peroxide sensitivity  
640 in agricultural soil dusts at temperatures  $> -18$  to  $-15$  °C, respectively, a range which aligns with  
641 the peroxide sensitivity exhibited in the present study.

642 Organic material can condense or adsorb onto aerosols during photochemical and oxidative  
643 processes, representing another potential source of organic INPs during AQABA (Dall’Osto et al.,  
644 2010; Hinz et al., 2005; Krueger et al., 2004). Could aging explain the organics and decreased  $n_s$   
645 observed? Though dust aerosol was collected within 1 day’s transport from source regions  
646 throughout this study, we cannot rule out the possibility of aging impacts, lacking single particle  
647 chemistry measurements. In addition to field observations of  $n_{\text{INP}}$  demonstrating that aging  
648 increased the IN efficiency of desert dust INPs (see Introduction; Boose et al., 2016; Conen et al.  
649 2015), prior studies of the effects of aging on mineral dust INPs have yielded mixed and sometimes  
650 contradictory results, indicating that the impact of aging on IN properties likely depends on  
651 multiple factors including the ice nucleation pathway, the type of aging process, surface  
652 morphology, and mineralogy (Perkins et al., 2020 and references therein). Multiple studies have  
653 investigated the effects of various aging processes on Arizona Test Dust (ATD) as a proxy for  
654 diverse natural dust samples. These included exposure to sulfuric acid, nitric acid vapor, and  
655 solution-phase processes (Cziczo et al., 2009; Eastwood et al., 2009; Knopf and Koop, 2006;  
656 Salam et al., 2007; Sullivan et al., 2010b, 2010a). Perkins et al. (2020) demonstrated the INP  
657 lability in ATD through multiple solution-phase aging processes (e.g., incubation in water,  
658 exposure to acid or salt), with up to 1000× reductions in INP abundance at freezing temperatures  
659  $> 10$  °C. This result contrasts with the increase in IN activity attributed to aging reported in Boose  
660 et al. (2016) and Conen et al. (2015). Perkins et al. (2020) additionally reported that the lability of  
661 IN activity in ATD is temperature dependent, with large reductions evident at freezing temperature  
662  $> 10$  °C, yet little to no change at temperatures  $< -15$  °C. By contrast, most of the  $n_s$  spectra in  
663 AQABA samples were 10 – 1000× lower than established dust parameterizations even at  
664 temperatures  $< -15$  °C. In summary, it has proven difficult to determine any consistent impact of  
665 atmospheric processing on the IN activity of dust in model systems such as ATD (Perkins et al.,  
666 2020), and few studies have investigated impacts of aging on ambient desert dust, especially at

667 modest supercooling (Boose et al., 2016). Furthermore, the use of ATD as a proxy for natural dust  
668 in INP studies has been questioned due to the complex ice-nucleating properties of natural dust,  
669 including mineral composition and defect sites at the particle surface, the latter of which is likely  
670 affected by the mechanical processing and milling involved in ATD production (e.g., Perkins et  
671 al., 2020 and references therein).

672 Gong et al. (2020) also observed  $n_s$  lower by more than 2 orders of magnitude compared to N12  
673 and U17 despite the large fraction of supermicron INPs (77-83% depending on temperature), and  
674 that the supermicron particles were mainly mineral dust. The cause of the decreased  $n_s$  observed  
675 here and in Gong et al. (2020) compared to dust  $n_s$  parameterizations remains elusive. Both studies  
676 were conducted in air masses dominated by dust near major sources. In contrast, Price et al. (2018)  
677 found agreement near the region of the Gong et al. (2020) study. One obvious difference is that  
678 Price et al. (2018) conducted measurements at higher altitudes, between 30 and 3500 m. A prior  
679 study that compared  $n_{\text{INP}}$  in dust-laden air masses at the surface with  $n_{\text{INP}}$  collected between 0.5  
680 and 3 km above sea level found that median  $n_{\text{INP}}$  increased by up to  $10\times$  above the surface and  
681 correlated to dust loading (Schrod et al., 2017). The differences between Price et al. (2018) and  
682 the two surface-based studies draws attention to the need for vertical profiles of  $n_s > -25$  °C in  
683 dust-laden air masses.

684 The decreased  $n_s$  compared to Price et al. (2018) is also unlikely to be related to differences in INP  
685 measurement. In all three studies, cold stage or droplet assay measurements of immersion mode  
686 INPs were used in resuspensions of aerosol collected on filter samples. Recent studies that  
687 intercompared instruments designed for measurement of immersion mode INPs showed excellent  
688 agreement (i.e., within measurement uncertainty) in measurements of standardized dust and  
689 biological samples (DeMott et al., 2018) and when co-sampling ambient aerosol (DeMott et al.,  
690 2017). Moreover, the DeMott et al. (2018) intercomparison study demonstrated good agreement  
691 in multiple natural dust samples between the various measurement methods used to derive D15,  
692 N12 and U17 and the droplet assay methods applied in Gong et al. (2020), Price et al. (2018), and  
693 the present study.

694 Storage protocol represents another difference between Price et al. (2018) and the two surface-  
695 based studies. Gong et al. (2020) and the present study stored samples frozen prior to analysis,

696 whereas Price et al. (2018) processed samples immediately after collection. An understanding of  
697 storage impacts on INPs collected on filters is lacking (Wex et al., 2019), but we note that the  
698 discrepancies in  $n_s$  between the two surface-based studies and Price et al. (2018) exceed the range  
699 of INP concentration changes reported in untreated INP precipitation samples stored frozen (Beall  
700 et al., 2020).

701 Thus, the large differences between parameterized  $n_s$  for dust, and  $n_s$  observed in both Gong et al.  
702 (2020) and the present study between -12 and -25 °C indicate that existing  $n_s$ -based  
703 parameterizations may not faithfully represent  $n_s$  at moderate freezing temperatures, despite  
704 proximity to major source regions. Whereas DeMott et al. (2015) found that for temperatures < -20  
705 °C, mineral dust particles from Saharan and Asian deserts may be parameterized as a common  
706 particle type, our findings suggest that characteristic  $n_s$  parameterizations for dust from different  
707 source regions may be needed > -20 °C, or, alternatively, that this temperature regime requires an  
708 alternative to an  $n_s$ -based parameterizations. Gong et al. (2019a) demonstrated that predicting  $n_{\text{INP}}$   
709 from surface area size distributions alone may not be feasible in environments where the aerosol  
710 and/or INP composition are unknown and proposed a probability density function (PDF)-based  
711 approach to predicting INPs at a given freezing temperature.

712 In light of the evidence from this study that INPs were primarily influenced by organics associated  
713 with dust, especially at higher temperatures, and the lack of relationship between dust loading,  $n_s$ ,  
714 and  $n_{\text{INP}}$ , we offer the following points for consideration. Prior studies of aerosolized dust  
715 demonstrated that it is frequently enriched in organic matter (6-20×) compared to soil dust and that  
716 wind erosion selectively removes the chemically-enriched, fine portion of the soil higher in plant  
717 nutrients, organic matter and metals (Aryal et al., 2012; Delany and Zenchelsky, 1976; Van Pelt  
718 and Zobeck, 2007). Furthermore, a recent study that measured airborne concentrations of  
719 prokaryotic cells over the Red Sea characterized the region as a “global hot spot” with average  
720 concentrations of 155,000 ( $\pm$  65,000) cells  $\text{m}^{-3}$ , 19× higher than that over the subtropical and  
721 tropical open oceans (Mayol et al., 2014; Yahya et al., 2019). Yahya et al. (2019) demonstrated  
722 that the microbial loading was very likely related to the high concentrations of dust, as 99.9% of  
723 the cells were attached to dust particles. Organic and biological species have been shown to  
724 dominate IN activity at temperatures > ~-15 °C in many studies (e.g., Ladino et al., 2019;  
725 O’Sullivan et al., 2018, Kanji et al., 2017, and references therein). Thus, a faithful representation

726 of dust INPs may require two parameterizations: one for the IN activity dominated by minerals <  
727  $\sim -15$  °C such as D15, U17 and N12, and another for the dust-associated organics  $> \sim -15$  °C. As  
728 IN-active organics are limited compared to the IN-active mineral component of dust, we could  
729 expect an increase in  $n_s$  slope between warm and cold regimes. The apparent decreased  $n_s$  observed  
730 in this study between  $-18$  and  $-12$  °C could potentially be related to a plateau in  $n_s$  through the  
731 transition between the mineral and organic “modes” (see untreated samples in Figs. 5-6). This  
732 study underscores the need to characterize the IN-active organic species associated with dust from  
733 major source regions and to investigate the extent to which biological and/or organic particles  
734 contribute to INP populations in dust-laden air masses at high to moderate freezing temperatures  
735  $\geq -15$  °C.

## 736 **5 Conclusions**

737 Observations from the two-month AQABA campaign in the Mediterranean, Red Sea, Arabian Sea  
738 and Arabian Gulf are among the first INP measurements made in close proximity to the two largest  
739 dust sources globally: the Sahara and the Arabian Peninsula (Kok et al., 2021). Observed  $n_{\text{INP}}$   
740 measured in 26 aerosol samples spanned 2 orders of magnitude ( $5 \times 10^{-3}$  to  $5 \times 10^{-1}$  L<sup>-1</sup> at  $-15$  °C).

741 In summary, INPs observed during AQABA were very likely dominated by mineral dust with  
742 some additional contributions possibly from densely-populated and/or agricultural regions  
743 including the Nile River Delta region and Southern or Eastern Europe. Despite proximity to major  
744 dust sources and a high frequency of dust events with MERRA-2 simulated mass concentrations  
745 up to  $490 \mu\text{g m}^{-3}$  (PM<sub>10</sub>), the observed  $n_s$  for most samples was lower by 1-3 orders of magnitude  
746 compared to  $n_s$  predicted by dust parametrizations N12 and U17 at  $T < -12$  °C. Observed  $n_s$  for  
747 some samples was equivalent to that of the A13 parameterization for K-feldspar (Atkinson et al.,  
748 2013), an ice-active component of desert dust, observations within the marine boundary layer  
749 (DeMott et al., 2016; Yang et al., 2020), and Price et al.'s (2018) measurements of  $n_{\text{INP}}$  in dust-  
750 laden air masses over the Tropical Atlantic. Peroxide sensitivity was evident in all samples tested  
751 (12 of 26), at temperatures  $\geq -15$  °C, demonstrating a consistent contribution of organic material  
752 to warm-temperature INPs. Heat-sensitivity further suggested the presence of biological (e.g.,  
753 proteinaceous) INPs in a subset of samples, particularly at high freezing temperatures  $> -10$  °C. A  
754 soil dust sample from North Africa (originally from N12) exhibited heat and peroxide sensitivity

755 between -5 and -16 °C, further demonstrating that the IN activity of mineral dust could be  
756 associated with organic and/or biological material. Contrary to Price et al. (2018), who measured  
757 INP in the dust-laden Tropical Atlantic, no correlation was found between dust loading and  $n_{\text{INP}}$   
758 or  $n_s$ . Results from this study and Gong et al. (2020) indicate that the existing  $n_s$  parameterizations  
759 alone do not skillfully represent mineral dust associated INPs at modest supercooling near major  
760 dust sources.

761 The source strengths of Red Sea, Mediterranean, Arabian Sea, and Arabian Gulf bulk seawater  
762 were also evaluated. The maximum source potential was observed in the Arabian Sea (50 INP  
763  $\text{mL}^{-1}$  at -19 °C.) The observed  $n_{\text{INP}}$  for SSW samples were equivalent to those of Gong et al.  
764 (2020) at Cabo Verde within the 95% binomial sampling confidence intervals (Agresti and Coull,  
765 1998).

766 Considering that desert dust parameterizations overpredicted the  $n_s$  values observed during  
767 AQABA, despite proximity to major global emissions sources, this study demonstrates the need  
768 to evaluate the fidelity of dust INP parameterizations in nascent versus aged dust populations.  
769 The discrepancies underscore the challenges of evaluating dust-specific INP parameterizations:  
770 limited observations at modest supercooling, few assured methods for distinguishing between  
771 different INP sources in ambient aerosol, a dearth of characteristic soil dust samples from major  
772 dust sources, and limited knowledge of the specific composition and characteristics of dust INPs  
773 at temperatures  $> -15$  °C. Vertical profiles of  $n_s$  in dust-laden air masses are also needed to  
774 determine whether  $n_s$  is consistently lower at the surface and examine the variability of  $n_s$  with  
775 altitude. Potential storage impacts on INPs collected on filters are an additional factor worthy of  
776 future investigation, though storage alone does not likely explain the relatively decreased  $n_s$   
777 compared to parameterizations observed in this study, as U17 and N12 were both derived from  
778 stored dust samples.

779 In addition to providing observations at high to moderate freezing temperatures, future studies  
780 could apply the methods developed in Gong et al. (2020) to estimate the contribution of marine  
781 INPs to the aerosol sampled by assuming equivalent distributions of sea salt and INPs between  
782 seawater and air. Furthermore, given the combination of marine, dust, and anthropogenically-  
783 influenced air masses encountered, and the evidence of organic and biological INPs at modest  
784 supercooling in this study and Gong et al. (2020), future studies could benefit from advances in



785 on-line Light-Induced Fluorescence (LIF) measurement techniques. Whereas the interpretation of  
786 fluorescence data from most LIF-based instruments has been limited by the lack of spectroscopic  
787 information, newer instruments support real-time spectrally-resolved size and fluorescence  
788 measurement information for single particles (Fennelly et al., 2018; Huffman et al., 2020;  
789 Könemann et al., 2019). This information could be used to potentially “tag” different classes of  
790 organics and biological aerosols, enabling investigations of relationships between  $n_s$ ,  $n_{\text{INP}}$  and  
791 organic signatures in, e.g., mineral dusts and agricultural soil dusts. Finally, the decreased  $n_s$   
792 observed in this study further motivate comprehensive aerosol-ice nucleation studies, which aim  
793 to achieve closure between measured and predicted ambient  $n_{\text{INP}}$  by simultaneously characterizing  
794 ambient INPs and ice nucleation relevant properties of the total aerosol population, such as  
795 composition and aerosol chemical mixing state (Sullivan et al., 2007).

796 **Data Availability:** The data set supporting this manuscript is hosted by the UCSD Library  
797 Digital Collections (<https://doi.org/10.6075/J0X0676P>) (Beall et al., 2021).

798 **Author contributions:**

799 CMB, TCH, PJD, MOA, CP, JL, JS, FD, BW, HH, MDS, and KAP designed the study. CMB  
800 performed the INP measurements, FLEXPART modeling and analysis with support from TCH,  
801 PJD, MOA, MDS, MP and KAP. TCH, PJD and MOA contributed significantly to the writing,  
802 preparation of figures and analysis. TK, MI, RP and HH supported the field collection of aerosol  
803 for INP analysis and TK additionally provided aerosol number concentration data. JS and MP  
804 provided aerosol water-soluble composition data. FD oversaw the aerosol sizing and AMS  
805 composition measurements and analysis. All authors contributed to the writing of the article.

806 **Competing interests:**

807 The authors declare they have no conflict of interest.

808

809 **Acknowledgements:**

810 The authors acknowledge collaborations with King Abdullah University of Science and  
811 Technology (KAUST), the Cyprus Institute (CyI) and the Kuwait Institute for Scientific Research

812 (KISR). We additionally thank Marcel Dorf and Claus Koeppel for the organization of the  
813 campaign, as well as Horst Fischer, Ivan Tadic and Uwe Parchatka for provision of the NO data.  
814 Analyses and visualizations of dust mass concentrations and Chl *a* used in this paper were  
815 produced with the Giovanni online data system, developed and maintained by the NASA GES  
816 DISC. Maps throughout this article were created using ArcGIS® software by Esri. We would also  
817 like to thank Hays Ships Ltd. and the *Kommandor Iona*'s crew for their attention to the safety and  
818 well-being of the researchers. Finally, we thank the three anonymous reviewers whose insightful  
819 comments strengthened this paper. Funding was provided by Highly Cited Program at King Saud  
820 University and the Max Planck Society and the University of California San Diego (UCSD)  
821 Understanding and Protecting the Planet initiative.

## 822 **References**

- 823 Agresti, A. and Coull, B. A.: Approximate Is Better than “Exact” for Interval Estimation of Binomial  
824 Proportions, *Am. Stat.*, 52(2), 119, doi:10.2307/2685469, 1998.
- 825 Ardon-Dryer, K. and Levin, Z.: Ground-based measurements of immersion freezing in the eastern  
826 Mediterranean, *Atmos. Chem. Phys.*, 14(10), 5217–5231, doi:10.5194/acp-14-5217-2014, 2014.
- 827 Aryal, R., Kandel, D., Acharya, D., Chong, M. N. and Beecham, S.: Unusual Sydney dust storm and its  
828 mineralogical and organic characteristics, *Environ. Chem.*, 9(6), 537–546 [online] Available from:  
829 <https://doi.org/10.1071/EN12131>, 2012.
- 830 Atkinson, J. D., Murray, B. J., Woodhouse, M. T., Whale, T. F., Baustian, K. J., Carslaw, K. S., Dobbie,  
831 S., O’Sullivan, D. and Malkin, T. L.: The importance of feldspar for ice nucleation by mineral dust in  
832 mixed-phase clouds, *Nature*, 498(7454), 355–358, doi:10.1038/nature12278, 2013.
- 833 Beall, C. M., Stokes, M. D., Hill, T. C., DeMott, P. J., DeWald, J. T. and Prather, K. A.: Automation and  
834 Heat Transfer Characterization of Immersion Mode Spectroscopy for Analysis of Ice Nucleating  
835 Particles, *Atmos. Meas. Tech.*, (February), 1–25, doi:10.5194/amt-2016-412, 2017.
- 836 Beall, C. M., Lucero, D., Hill, T. C., DeMott, P. J., Stokes, M. D. and Prather, K. A.: Best practices for  
837 precipitation sample storage for offline studies of ice nucleation in marine and coastal environments,  
838 *Atmos. Meas. Tech.*, 13(12), 6473–6486, doi:10.5194/amt-13-6473-2020, 2020.
- 839 Beall, C. M., Michaud, J. M., Fish, M. A., Dinasquet, J., Cornwell, G. C., Stokes, M. D., Burkart, M. D.,  
840 Hill, T. C., Demott, P. J. and Prather, K. A.: Cultivable halotolerant ice-nucleating bacteria and fungi in  
841 coastal precipitation, *Atmos. Chem. Phys.*, 21(11), 9031–9045, doi:10.5194/acp-21-9031-2021, 2021.

842 Boose, Y., Sierau, B., Isabel García, M., Rodríguez, S., Alastuey, A., Linke, C., Schnaiter, M.,  
843 Kupiszewski, P., Kanji, Z. A. and Lohmann, U.: Ice nucleating particles in the Saharan Air Layer, *Atmos.*  
844 *Chem. Phys.*, 16(14), 9067–9087, doi:10.5194/acp-16-9067-2016, 2016.

845 Boose, Y., Baloh, P., Plötze, M., Ofner, J., Grothe, H., Sierau, B., Lohmann, U. and Kanji, Z. A.:  
846 Heterogeneous ice nucleation on dust particles sourced from nine deserts worldwide -- Part 2: Deposition  
847 nucleation and condensation freezing, *Atmos. Chem. Phys.*, 19(2), 1059–1076, doi:10.5194/acp-19-1059-  
848 2019, 2019.

849 Bourtsoukidis, E., Ernle, L., Crowley, J. N., Lelieveld, J., Paris, J.-D., Pozzer, A., Walter, D. and  
850 Williams, J.: Non-methane hydrocarbon ( $\text{C}_2$ – $\text{C}_8$ ) sources and sinks around the  
851 Arabian Peninsula, *Atmos. Chem. Phys.*, 19(10), 7209–7232, doi:10.5194/acp-19-7209-2019, 2019.

852 Bourtsoukidis, E., Pozzer, A., Sattler, T., Matthaios, V. N., Ernle, L., Edtbauer, A., Fischer, H.,  
853 Könemann, T., Osipov, S., Paris, J.-D., Pfannerstill, E. Y., Stöner, C., Tadic, I., Walter, D., Wang, N.,  
854 Lelieveld, J. and Williams, J.: The Red Sea Deep Water is a potent source of atmospheric ethane and  
855 propane, *Nat. Commun.*, 11(1), 447, doi:10.1038/s41467-020-14375-0, 2020.

856 Broadley, S. L., Murray, B. J., Herbert, R. J., Atkinson, J. D., Dobbie, S., Malkin, T. L., Condliffe, E. and  
857 Neve, L.: Immersion mode heterogeneous ice nucleation by an illite rich powder representative of  
858 atmospheric mineral dust, *Atmos. Chem. Phys.*, 12(1), 287–307, doi:10.5194/acp-12-287-2012, 2012.

859 Brunner, C., Brem, B. T., Collaud Coen, M., Conen, F., Hervo, M., Henne, S., Steinbacher, M., Gysel-  
860 Beer, M. and Kanji, Z. A.: The contribution of Saharan dust to the ice-nucleating particle concentrations  
861 at the High Altitude Station Jungfraujoch (3580 m a.s.l.), Switzerland, *Atmos. Chem. Phys.*, 21(23),  
862 18029–18053, doi:10.5194/acp-21-18029-2021, 2021.

863 Buchard, V., Randles, C. A., da Silva, A. M., Darmenov, A., Colarco, P. R., Govindaraju, R., Ferrare, R.,  
864 Hair, J., Beyersdorf, A. J., Ziemba, L. D. and Yu, H.: The MERRA-2 Aerosol Reanalysis, 1980 Onward.  
865 Part II: Evaluation and Case Studies, *J. Clim.*, 30(17), 6851–6872, doi:10.1175/JCLI-D-16-0613.1, 2017.

866 Burrows, S. M., Hoose, C., Pöschl, U. and Lawrence, M. G.: Ice nuclei in marine air: biogenic particles or  
867 dust?, *Atmos. Chem. Phys.*, 13(1), 245–267, doi:10.5194/acp-13-245-2013, 2013.

868 Celik, S., Drewnick, F., Fachinger, F., Brooks, J., Darbyshire, E., Coe, H., Paris, J.-D., Eger, P. G.,  
869 Schuladen, J., Tadic, I., Friedrich, N., Dienhart, D., Hottmann, B., Fischer, H., Crowley, J. N., Harder, H.  
870 and Borrmann, S.: Influence of vessel characteristics and atmospheric processes on the gas and particle  
871 phase of ship emission plumes: in situ measurements in the Mediterranean Sea and around the Arabian  
872 Peninsula, *Atmos. Chem. Phys.*, 20(8), 4713–4734, doi:10.5194/acp-20-4713-2020, 2020.

873 Collins, D. B., Zhao, D. F., Ruppel, M. J., Laskina, O., Grandquist, J. R., Modini, R. L., Stokes, M. D.,  
874 Russell, L. M., Bertram, T. H., Grassian, V. H., Deane, G. B. and Prather, K. A.: Direct aerosol chemical  
875 composition measurements to evaluate the physicochemical differences between controlled sea spray  
876 aerosol generation schemes, *Atmos. Meas. Tech.*, 7(11), 3667–3683, doi:10.5194/amt-7-3667-2014,  
877 2014.

878 Conen, F., Morris, C. E., Leifeld, J., Yakutin, M. V and Alewell, C.: Biological residues define the ice  
879 nucleation properties of soil dust, *Atmos. Chem. Phys.*, 11(18), 9643–9648, doi:10.5194/acp-11-9643-  
880 2011, 2011.

881 Conen, F., Rodríguez, S., Hüglin, C., Henne, S., Herrmann, E., Bukowiecki, N. and Alewell, C.:  
882 Atmospheric ice nuclei at the high-altitude observatory Jungfraujoch, Switzerland, *Tellus, Ser. B Chem.*  
883 *Phys. Meteorol.*, 67(1), 1–10, doi:10.3402/tellusb.v67.25014, 2015.

884 Conen, F., Einbock, A., Mignani, C. and Hüglin, C.: Measurement report: Ice-nucleating particles active  
885  $-15^{\circ}\text{C}$  in free tropospheric air over western Europe, *Atmos. Chem. Phys.*, 22(5), 3433–  
886 3444, doi:10.5194/acp-22-3433-2022, 2022.

887 Cornwell, G. C., McCluskey, C. S., Levin, E. J. T., Suski, K. J., DeMott, P. J., Kreidenweis, S. M. and  
888 Prather, K. A.: Direct Online Mass Spectrometry Measurements of Ice Nucleating Particles at a California  
889 Coastal Site, *J. Geophys. Res. Atmos.*, 124(22), 12157–12172, doi:doi:10.1029/2019JD030466, 2019.

890 Cornwell, G. C., Sultana, C. M., Prank, M., Cochran, R. E., Hill, T. C. J., Schill, G. P., DeMott, P. J.,  
891 Mahowald, N. and Prather, K. A.: Ejection of Dust From the Ocean as a Potential Source of Marine Ice  
892 Nucleating Particles, *J. Geophys. Res. Atmos.*, 125(24), e2020JD033073,  
893 doi:https://doi.org/10.1029/2020JD033073, 2020.

894 Cziczo, D. J., Froyd, K. D., Gallavardin, S. J., Moehler, O., Benz, S., Saathoff, H. and Murphy, D. M.:  
895 Deactivation of ice nuclei due to atmospherically relevant surface coatings, *Environ. Res. Lett.*, 4(4),  
896 44013, doi:10.1088/1748-9326/4/4/044013, 2009.

897 Dall’Osto, M., Harrison, R. M., Highwood, E. J., O’Dowd, C., Ceburnis, D., Querol, X. and Achterberg,  
898 E. P.: Variation of the mixing state of Saharan dust particles with atmospheric transport, *Atmos. Environ.*,  
899 44(26), 3135–3146, doi:https://doi.org/10.1016/j.atmosenv.2010.05.030, 2010.

900 Delany, A. C. and Zenchelsky, S.: THE ORGANIC COMPONENT OF WIND-EROSION-  
901 GENERATED SOIL-DERIVED AEROSOL, *Soil Sci.*, 121(3) [online] Available from:  
902 [https://journals.lww.com/soilsci/Fulltext/1976/03000/THE\\_ORGANIC\\_COMPONENT\\_OF\\_WIND\\_ER](https://journals.lww.com/soilsci/Fulltext/1976/03000/THE_ORGANIC_COMPONENT_OF_WIND_EROSION_GENERATED.2.aspx)  
903 [OSION\\_GENERATED.2.aspx](https://journals.lww.com/soilsci/Fulltext/1976/03000/THE_ORGANIC_COMPONENT_OF_WIND_EROSION_GENERATED.2.aspx), 1976.

904 Demott, P. J., Prenni, A. J., Mcmeeking, G. R., Sullivan, R. C., Petters, M. D., Tobo, Y., Niemand, M.,  
905 Möhler, O., Snider, J. R., Wang, Z. and Kreiden: Integrating laboratory and field data to quantify the  
906 immersion freezing ice nucleation activity of mineral dust particles, , 393–409, doi:10.5194/acp-15-393-  
907 2015, 2015.

908 DeMott, P. J., Hill, T. C. J., McCluskey, C. S., Prather, K. A., Collins, D. B., Sullivan, R. C., Ruppel, M.  
909 J., Mason, R. H., Irish, V. E., Lee, T., Hwang, C. Y., Rhee, T. S., Snider, J. R., McMeeking, G. R.,  
910 Dhaniyala, S., Lewis, E. R., Wentzell, J. J. B., Abbatt, J., Lee, C., Sultana, C. M., Ault, A. P., Axson, J.  
911 L., Diaz Martinez, M., Venero, I., Santos-Figueroa, G., Stokes, M. D., Deane, G. B., Mayol-Bracero, O.  
912 L., Grassian, V. H., Bertram, T. H., Bertram, A. K., Moffett, B. F. and Franc, G. D.: Sea spray aerosol as  
913 a unique source of ice nucleating particles, *Proc. Natl. Acad. Sci.*, 113(21), 5797–5803,  
914 doi:10.1073/pnas.1514034112, 2016.

915 DeMott, P. J., Hill, T. C. J., Petters, M. D., Bertram, A. K., Tobo, Y., Mason, R. H., Suski, K. J.,  
916 McCluskey, C. S., Levin, E. J. T., Schill, G. P., Boose, Y., Rauker, A. M., Miller, A. J., Zaragoza, J.,  
917 Rocci, K., Rothfuss, N. E., Taylor, H. P., Hader, J. D., Chou, C., Huffman, J. A., Pöschl, U., Prenni, A. J.  
918 and Kreidenweis, S. M.: Comparative measurements of ambient atmospheric concentrations of ice  
919 nucleating particles using multiple immersion freezing methods and a continuous flow diffusion chamber,  
920 *Atmos. Chem. Phys.*, 17(18), 11227–11245, doi:10.5194/acp-17-11227-2017, 2017.

921 DeMott, P. J., Möhler, O., Cziczo, D. J., Hiranuma, N., Petters, M. D., Petters, S. S., Belosi, F.,  
922 Bingemer, H. G., Brooks, S. D., Budke, C., Burkert-Kohn, M., Collier, K. N., Danielczok, A., Eppers, O.,  
923 Felgitsch, L., Garimella, S., Grothe, H., Herenz, P., Hill, T. C. J., Höhler, K., Kanji, Z. A., Kiselev, A.,  
924 Koop, T., Kristensen, T. B., Krüger, K., Kulkarni, G., Levin, E. J. T., Murray, B. J., Nicosia, A.,  
925 O’Sullivan, D., Peckhaus, A., Polen, M. J., Price, H. C., Reicher, N., Rothenberg, D. A., Rudich, Y.,  
926 Santachiara, G., Schiebel, T., Schrod, J., Seifried, T. M., Stratmann, F., Sullivan, R. C., Suski, K. J.,  
927 Szakáll, M., Taylor, H. P., Ullrich, R., Vergara-Temprado, J., Wagner, R., Whale, T. F., Weber, D., Welti,  
928 A., Wilson, T. W., Wolf, M. J. and Zenker, J.: The Fifth International Workshop on Ice Nucleation phase  
929 2 (FIN-02): laboratory intercomparison of ice nucleation measurements, *Atmos. Meas. Tech.*, 11(11),  
930 6231–6257, doi:10.5194/amt-11-6231-2018, 2018.

931 Eastwood, M. L., Cremel, S., Wheeler, M., Murray, B. J., Girard, E. and Bertram, A. K.: Effects of  
932 sulfuric acid and ammonium sulfate coatings on the ice nucleation properties of kaolinite particles,  
933 *Geophys. Res. Lett.*, 36(2), doi:<https://doi.org/10.1029/2008GL035997>, 2009.

934 Edtbauer, A., Stöner, C., Pfannerstill, E. Y., Berasategui, M., Walter, D., Crowley, J. N., Lelieveld, J.  
935 and Williams, J.: A new marine biogenic emission: methane sulfonamide (MSAM), dimethyl sulfide

936 (DMS), and dimethyl sulfone ( $\text{chem}\{\text{DMSO}_{2}\}$ ) measured in air over the Arabian Sea, *Atmos. Chem.*  
937 *Phys.*, 20(10), 6081–6094, doi:10.5194/acp-20-6081-2020, 2020.

938 Eger, P. G., Friedrich, N., Schuladen, J., Shenolikar, J., Fischer, H., Tadic, I., Harder, H., Martinez, M.,  
939 Rohloff, R., Tauer, S., Drewnick, F., Fachinger, F., Brooks, J., Darbyshire, E., Sciare, J., Pikridas, M.,  
940 Lelieveld, J. and Crowley, J. N.: Shipborne measurements of  $\text{ClNO}_{2}$  in the Mediterranean Sea and  
941 around the Arabian Peninsula during summer, *Atmos. Chem. Phys.*, 19(19), 12121–12140,  
942 doi:10.5194/acp-19-12121-2019, 2019.

943 Fennelly, M. J., Sewell, G., Prentice, M. B., O’Connor, D. J. and Sodeau, J. R.: Review: The Use of Real-  
944 Time Fluorescence Instrumentation to Monitor Ambient Primary Biological Aerosol Particles (PBAP),  
945 *Atmosphere (Basel)*, 9(1), doi:10.3390/atmos9010001, 2018.

946 Friedrich, N., Eger, P., Shenolikar, J., Sobanski, N., Schuladen, J., Dienhart, D., Hottmann, B., Tadic, I.,  
947 Fischer, H., Martinez, M., Rohloff, R., Tauer, S., Harder, H., Pfannerstill, E. Y., Wang, N., Williams, J.,  
948 Brooks, J., Drewnick, F., Su, H., Li, G., Cheng, Y., Lelieveld, J. and Crowley, J. N.: Reactive nitrogen  
949 around the Arabian Peninsula and in the Mediterranean Sea during the 2017 AQABA ship campaign,  
950 *Atmos. Chem. Phys.*, 21(10), 7473–7498, doi:10.5194/acp-21-7473-2021, 2021.

951 Gandham, H., Dasari, H. P., Langodan, S., Karumuri, R. K. and Hoteit, I.: Major Changes in Extreme  
952 Dust Events Dynamics Over the Arabian Peninsula During 2003–2017 Driven by Atmospheric  
953 Conditions, *J. Geophys. Res. Atmos.*, 125(24), e2020JD032931,  
954 doi:https://doi.org/10.1029/2020JD032931, 2020.

955 Gelaro, R., McCarty, W., Suárez, M. J., Todling, R., Molod, A., Takacs, L., Randles, C. A., Darmenov,  
956 A., Bosilovich, M. G., Reichle, R., Wargan, K., Coy, L., Cullather, R., Draper, C., Akella, S., Buchard,  
957 V., Conaty, A., da Silva, A. M., Gu, W., Kim, G.-K., Koster, R., Lucchesi, R., Merkova, D., Nielsen, J.  
958 E., Partyka, G., Pawson, S., Putman, W., Rienecker, M., Schubert, S. D., Sienkiewicz, M. and Zhao, B.:  
959 The Modern-Era Retrospective Analysis for Research and Applications, Version 2 (MERRA-2), *J. Clim.*,  
960 30(14), 5419–5454, doi:10.1175/JCLI-D-16-0758.1, 2017.

961 Gong, X., Wex, H., Müller, T., Wiedensohler, A., Höhler, K., Kandler, K., Ma, N., Dietel, B., Schiebel,  
962 T., Möhler, O. and Stratmann, F.: Characterization of aerosol properties at Cyprus, focusing on cloud  
963 condensation nuclei and ice-nucleating particles, *Atmos. Chem. Phys.*, 19(16), 10883–10900,  
964 doi:10.5194/acp-19-10883-2019, 2019a.

965 Gong, X., Wex, H., van Pinxteren, M., Triesch, N., Fomba, K. W., Lubitz, J., Stolle, C., Robinson, T.-B.,  
966 Müller, T., Herrmann, H. and Stratmann, F.: Ice nucleating particles measured in air, cloud and seawater

967 at the Cape Verde Atmospheric Observatory (CVAO), , doi:10.1594/PANGAEA.906946, 2019b.

968 Gong, X., Wex, H., van Pinxteren, M., Triesch, N., Fomba, K. W., Lubitz, J., Stolle, C., Robinson, T.-B.,  
969 Müller, T., Herrmann, H. and Stratmann, F.: Characterization of aerosol particles at Cabo Verde close to  
970 sea level and at the cloud level -- Part 2: Ice-nucleating particles in air, cloud and seawater, *Atmos. Chem.*  
971 *Phys.*, 20(3), 1451–1468, doi:10.5194/acp-20-1451-2020, 2020.

972 Hara, K., Maki, T., Kakikawa, M., Kobayashi, F. and Matsuki, A.: Effects of different temperature  
973 treatments on biological ice nuclei in snow samples, *Atmos. Environ.*, 140, 415–419,  
974 doi:10.1016/j.atmosenv.2016.06.011, 2016.

975 Harrison, A. D., Whale, T. F., Carpenter, M. A., Holden, M. A., Neve, L., O’Sullivan, D., Vergara  
976 Temprado, J. and Murray, B. J.: Not all feldspars are equal: a survey of ice nucleating properties across  
977 the feldspar group of minerals, *Atmos. Chem. Phys.*, 16(17), 10927–10940, doi:10.5194/acp-16-10927-  
978 2016, 2016.

979 Harrison, A. D., Lever, K., Sanchez-Marroquin, A., Holden, M. A., Whale, T. F., Tarn, M. D., McQuaid,  
980 J. B. and Murray, B. J.: The ice-nucleating ability of quartz immersed in water and its atmospheric  
981 importance compared to K-feldspar, *Atmos. Chem. Phys.*, 19(17), 11343–11361, doi:10.5194/acp-19-  
982 11343-2019, 2019.

983 Hartmann, M., Adachi, K., Eppers, O., Haas, C., Herber, A., Holzinger, R., Hünerbein, A., Jäkel, E.,  
984 Jentsch, C., van Pinxteren, M., Wex, H., Willmes, S. and Stratmann, F.: Wintertime Airborne  
985 Measurements of Ice Nucleating Particles in the High Arctic: A Hint to a Marine, Biogenic Source for Ice  
986 Nucleating Particles, *Geophys. Res. Lett.*, 47(13), e2020GL087770,  
987 doi:https://doi.org/10.1029/2020GL087770, 2020.

988 Hill, T. C. J., DeMott, P. J., Tobo, Y., Fröhlich-Nowoisky, J., Moffett, B. F., Franc, G. D. and  
989 Kreidenweis, S. M.: Sources of organic ice nucleating particles in soils, *Atmos. Chem. Phys.*, 16(11),  
990 7195–7211, doi:10.5194/acp-16-7195-2016, 2016.

991 Hinz, K.-P., Trimborn, A., Weingartner, E., Henning, S., Baltensperger, U. and Spengler, B.: Aerosol  
992 single particle composition at the Jungfrauoch, *J. Aerosol Sci.*, 36(1), 123–145,  
993 doi:https://doi.org/10.1016/j.jaerosci.2004.08.001, 2005.

994 Hiranuma, N., Augustin-Bauditz, S., Bingemer, H., Budke, C., Curtius, J., Danielczok, A., Diehl, K.,  
995 Dreischmeier, K., Ebert, M., Frank, F., Hoffmann, N., Kandler, K., Kiselev, A., Koop, T., Leisner, T.,  
996 Möhler, O., Nillius, B., Peckhaus, A., Rose, D., Weinbruch, S., Wex, H., Boose, Y., DeMott, P. J., Hader,  
997 J. D., Hill, T. C. J., Kanji, Z. A., Kulkarni, G., Levin, E. J. T., McCluskey, C. S., Murakami, M., Murray,

998 B. J., Niedermeier, D., Petters, M. D., O’Sullivan, D., Saito, A., Schill, G. P., Tajiri, T., Tolbert, M. A.,  
999 Welti, A., Whale, T. F., Wright, T. P. and Yamashita, K.: A comprehensive laboratory study on the  
1000 immersion freezing behavior of illite NX particles: a comparison of 17 ice nucleation measurement  
1001 techniques, *Atmos. Chem. Phys.*, 15(5), 2489–2518, doi:10.5194/acp-15-2489-2015, 2015.

1002 Hoose, C. and Möhler, O.: Heterogeneous ice nucleation on atmospheric aerosols: A review of results  
1003 from laboratory experiments., 2012.

1004 Hoose, C., Kristjánsson, J. E., Chen, J.-P. and Hazra, A.: A Classical-Theory-Based Parameterization of  
1005 Heterogeneous Ice Nucleation by Mineral Dust, Soot, and Biological Particles in a Global Climate Model,  
1006 *J. Atmos. Sci.*, 67(8), 2483–2503, doi:10.1175/2010JAS3425.1, 2010.

1007 Huffman, J. A., Perring, A. E., Savage, N. J., Clot, B., Crouzy, B., Tummon, F., Shoshanim, O., Damit,  
1008 B., Schneider, J., Sivaprakasam, V., Zawadowicz, M. A., Crawford, I., Gallagher, M., Topping, D.,  
1009 Doughty, D. C., Hill, S. C. and Pan, Y.: Real-time sensing of bioaerosols: Review and current  
1010 perspectives, *Aerosol Sci. Technol.*, 54(5), 465–495, doi:10.1080/02786826.2019.1664724, 2020.

1011 Huneus, N., Schulz, M., Balkanski, Y., Griesfeller, J., Prospero, J., Kinne, S., Bauer, S., Boucher, O.,  
1012 Chin, M., Dentener, F., Diehl, T., Easter, R., Fillmore, D., Ghan, S., Ginoux, P., Grini, A., Horowitz, L.,  
1013 Koch, D., Krol, M. C., Landing, W., Liu, X., Mahowald, N., Miller, R., Morcrette, J.-J., Myhre, G.,  
1014 Penner, J., Perlwitz, J., Stier, P., Takemura, T. and Zender, C. S.: Global dust model intercomparison in  
1015 AeroCom phase I, *Atmos. Chem. Phys.*, 11(15), 7781–7816, doi:10.5194/acp-11-7781-2011, 2011.

1016 Kanji, Z. A., Ladino, L. A., Wex, H., Boose, Y., Burkert-Kohn, M., Cziczo, D. J. and Krämer, M.:  
1017 Overview of Ice Nucleating Particles, *Meteorol. Monogr.*, 58, 1.1-1.33, doi:10.1175/amsmonographs-d-  
1018 16-0006.1, 2017.

1019 Khaniabadi, Y. O., Daryanoosh, S. M., Amrane, A., Polosa, R., Hopke, P. K., Goudarzi, G., Mohammadi,  
1020 M. J., Sicard, P. and Armin, H.: Impact of Middle Eastern Dust storms on human health, *Atmos. Pollut.*  
1021 *Res.*, 8(4), 606–613, doi:https://doi.org/10.1016/j.apr.2016.11.005, 2017.

1022 Kinne, S., Schulz, M., Textor, C., Guibert, S., Balkanski, Y., Bauer, S. E., Berntsen, T., Berglen, T. F.,  
1023 Boucher, O., Chin, M., Collins, W., Dentener, F., Diehl, T., Easter, R., Feichter, J., Fillmore, D., Ghan,  
1024 S., Ginoux, P., Gong, S., Grini, A., Hendricks, J., Herzog, M., Horowitz, L., Isaksen, I., Iversen, T.,  
1025 Kirkevåg, A., Kloster, S., Koch, D., Kristjansson, J. E., Krol, M., Lauer, A., Lamarque, J. F., Lesins, G.,  
1026 Liu, X., Lohmann, U., Montanaro, V., Myhre, G., Penner, J., Pitari, G., Reddy, S., Seland, O., Stier, P.,  
1027 Takemura, T. and Tie, X.: An AeroCom initial assessment – optical properties in aerosol component  
1028 modules of global models, *Atmos. Chem. Phys.*, 6(7), 1815–1834, doi:10.5194/acp-6-1815-2006, 2006.



1029 Kleist, D. T., Parrish, D. F., Derber, J. C., Treadon, R., Wu, W.-S. and Lord, S.: Introduction of the GSI  
1030 into the NCEP Global Data Assimilation System, *Weather Forecast.*, 24(6), 1691–1705,  
1031 doi:10.1175/2009WAF2222201.1, 2009.

1032 Klingmüller, K., Pozzer, A., Metzger, S., Stenchikov, G. L. and Lelieveld, J.: Aerosol optical depth trend  
1033 over the Middle East, *Atmos. Chem. Phys.*, 16(8), 5063–5073, doi:10.5194/acp-16-5063-2016, 2016.

1034 Knopf, D. A. and Koop, T.: Heterogeneous nucleation of ice on surrogates of mineral dust, *J. Geophys.*  
1035 *Res. Atmos.*, 111(D12), doi:https://doi.org/10.1029/2005JD006894, 2006.

1036 Kok, J. F., Adebisi, A. A., Albani, S., Balkanski, Y., Checa-Garcia, R., Chin, M., Colarco, P. R.,  
1037 Hamilton, D. S., Huang, Y., Ito, A., Klose, M., Li, L., Mahowald, N. M., Miller, R. L., Obiso, V., Pérez  
1038 Garc\'ia-Pando, C., Rocha-Lima, A. and Wan, J. S.: Contribution of the world's main dust source regions  
1039 to the global cycle of desert dust, *Atmos. Chem. Phys.*, 21(10), 8169–8193, doi:10.5194/acp-21-8169-  
1040 2021, 2021.

1041 Könemann, T., Savage, N., Klimach, T., Walter, D., Fröhlich-Nowoisky, J., Su, H., Pöschl, U., Huffman,  
1042 J. A. and Pöhlker, C.: Spectral Intensity Bioaerosol Sensor (SIBS): an instrument for spectrally resolved  
1043 fluorescence detection of single particles in real time, *Atmos. Meas. Tech.*, 12(2), 1337–1363,  
1044 doi:10.5194/amt-12-1337-2019, 2019.

1045 Krasnov, H., Katra, I. and Friger, M.: Increase in dust storm related PM10 concentrations: A time series  
1046 analysis of 2001–2015, *Environ. Pollut.*, 213, 36–42, doi:https://doi.org/10.1016/j.envpol.2015.10.021,  
1047 2016.

1048 Krueger, B. J., Grassian, V. H., Cowin, J. P. and Laskin, A.: Heterogeneous chemistry of individual  
1049 mineral dust particles from different dust source regions: the importance of particle mineralogy, *Atmos.*  
1050 *Environ.*, 38(36), 6253–6261, doi:https://doi.org/10.1016/j.atmosenv.2004.07.010, 2004.

1051 Krzywinski, M. and Altman, N.: Error bars, *Nat. Methods*, 10(10), 921–922, doi:10.1038/nmeth.2659,  
1052 2013.

1053 Ladino, L. A., Raga, G. B., Alvarez-Ospina, H., Andino-Enr\'iquez, M. A., Rosas, I., Mart\'inez, L.,  
1054 Salinas, E., Miranda, J., Ram\'irez-D\'iaz, Z., Figueroa, B., Chou, C., Bertram, A. K., Quintana, E. T.,  
1055 Maldonado, L. A., Garc\'ia-Reynoso, A., Si, M. and Irish, V. E.: Ice-nucleating particles in a coastal  
1056 tropical site, *Atmos. Chem. Phys.*, 19(9), 6147–6165, doi:10.5194/acp-19-6147-2019, 2019.

1057 Lohmann, U. and Feichter, J.: Global indirect aerosol effects: a review, *Atmos. Chem. Phys.*, 5(3), 715–  
1058 737, doi:10.5194/acp-5-715-2005, 2005.

1059 Manders, A. M. ., Schapp, M., Jozwicka, M., van Arkel, F., Weijers, E. . and Matthijsen, J.: The  
1060 contribution of sea salt to PM 10 and PM in the Netherlands, [online] Available from:  
1061 <http://www.pbl.nl/sites/default/files/cms/publicaties/500099004.pdf>, 2009.

1062 Martin, A. C., Cornwell, G., Beall, C. M., Cannon, F., Reilly, S., Schaap, B., Lucero, D., Creamean, J.,  
1063 Ralph, F. M., Mix, H. T. and Prather, K.: Contrasting local and long-range-transported warm ice-  
1064 nucleating particles during an atmospheric river in coastal California, USA, *Atmos. Chem. Phys.*, 19(7),  
1065 4193–4210, doi:10.5194/acp-19-4193-2019, 2019.

1066 Mayol, E., Jiménez, M. A., Herndl, G. J., Duarte, C. M. and Arrieta, J. M.: Resolving the abundance and  
1067 air-sea fluxes of airborne microorganisms in the North Atlantic Ocean, *Front. Microbiol.*, 5, 557,  
1068 doi:10.3389/fmicb.2014.00557, 2014.

1069 McCluskey, C. S., Hill, T. C. J., Malfatti, F., Sultana, C. M., Lee, C., Santander, M. V, Beall, C. M.,  
1070 Moore, K. A., Cornwell, G. C., Collins, D. B., Prather, K. A., Jayarathne, T., Stone, E. A., Azam, F.,  
1071 Kreidenweis, S. M. and DeMott, P. J.: A Dynamic Link between Ice Nucleating Particles Released in  
1072 Nascent Sea Spray Aerosol and Oceanic Biological Activity during Two Mesocosm Experiments, *J.*  
1073 *Atmos. Sci.*, 74(1), 151–166, doi:10.1175/JAS-D-16-0087.1, 2017.

1074 McCluskey, C. S., Hill, T. C. J., Sultana, C. M., Laskina, O., Trueblood, J., Santander, M. V., Beall, C.  
1075 M., Michaud, J. M., Kreidenweis, S. M., Prather, K. A., Grassian, V., DeMott, P. J., McCluskey, C. S.,  
1076 Hill, T. C. J., Sultana, C. M., Laskina, O., Trueblood, J., Santander, M. V., Beall, C. M., Michaud, J. M.,  
1077 Kreidenweis, S. M., Prather, K. A., Grassian, V. and DeMott, P. J.: A mesocosm double feature: Insights  
1078 into the chemical make-up of marine ice nucleating particles, *J. Atmos. Sci.*, JAS-D-17-0155.1,  
1079 doi:10.1175/JAS-D-17-0155.1, 2018a.

1080 McCluskey, C. S., Hill, T. C. J., Sultana, C. M., Laskina, O., Trueblood, J., Santander, M. V, Beall, C.  
1081 M., Michaud, J. M., Kreidenweis, S. M., Prather, K. A., Grassian, V. and DeMott, P. J.: A Mesocosm  
1082 Double Feature: Insights into the Chemical Makeup of Marine Ice Nucleating Particles, *J. Atmos. Sci.*,  
1083 75(7), 2405–2423, doi:10.1175/JAS-D-17-0155.1, 2018b.

1084 McCluskey, C. S., Ovadnevaite, J., Rinaldi, M., Atkinson, J., Belosi, F., Ceburnis, D., Marullo, S., Hill,  
1085 T. C. J., Lohmann, U., Kanji, Z. A., O’Dowd, C., Kreidenweis, S. M. and DeMott, P. J.: Marine and  
1086 Terrestrial Organic Ice-Nucleating Particles in Pristine Marine to Continentally Influenced Northeast  
1087 Atlantic Air Masses, *J. Geophys. Res. Atmos.*, 123(11), 6196–6212, doi:10.1029/2017JD028033, 2018c.

1088 McCluskey, C. S., Hill, T. C. J., Humphries, R. S., Rauker, A. M., Moreau, S., Stratton, P. G., Chambers,  
1089 S. D., Williams, A. G. and McRobert, I.: Observations of Ice Nucleating Particles Over Southern Ocean

1090 Waters, *Geophys. Res. Lett.*, 989–997, doi:10.1029/2018GL079981, 2018d.

1091 Mitts, B., Wang, X., Lucero, D., Beall, C., Deane, G., DeMott, P. and Prather, K.: Importance of  
1092 Supermicron Ice Nucleating Particles in Nascent Sea Spray, *Geophys. Res. Lett.*, n/a(n/a),  
1093 e2020GL089633, doi:https://doi.org/10.1029/2020GL089633, 2021.

1094 Molod, A., Takacs, L., Suarez, M. and Bacmeister, J.: Development of the GEOS-5 atmospheric general  
1095 circulation model: evolution from MERRA to MERRA2, *Geosci. Model Dev.*, 8(5), 1339–1356,  
1096 doi:10.5194/gmd-8-1339-2015, 2015.

1097 Murray, B. J., O’Sullivan, D., Atkinson, J. D. and Webb, M. E.: Ice nucleation by particles immersed in  
1098 supercooled cloud droplets., *Chem. Soc. Rev.*, 41(19), 6519–54, doi:10.1039/c2cs35200a, 2012.

1099 Nickovic, S., Vukovic, A., Vujadinovic, M., Djurdjevic, V. and Pejanovic, G.: Technical Note: High-  
1100 resolution mineralogical database of dust-productive soils for atmospheric dust modeling, *Atmos. Chem.*  
1101 *Phys.*, 12(2), 845–855, doi:10.5194/acp-12-845-2012, 2012.

1102 Niedermeier, D., Augustin-Bauditz, S., Hartmann, S., Wex, H., Ignatius, K. and Stratmann, F.: Can we  
1103 define an asymptotic value for the ice active surface site density for heterogeneous ice nucleation?, *J.*  
1104 *Geophys. Res. Atmos.*, 120(10), 5036–5046, doi:https://doi.org/10.1002/2014JD022814, 2015.

1105 Niemand, M., Möhler, O., Vogel, B., Vogel, H., Hoose, C., Connolly, P., Klein, H., Bingemer, H.,  
1106 Demott, P., Skrotzki, J. and Leisner, T.: A particle-surface-area-based parameterization of immersion  
1107 freezing on desert dust particles, *J. Atmos. Sci.*, 69(10), 3077–3092, doi:10.1175/JAS-D-11-0249.1, 2012.

1108 Nortcliff, S.: *World Soil Resources and Food Security*. Edited by R. Lal and BA Stewart. Boca Raton, FL,  
1109 USA: CRC Press (2012), pp. 574,£82.00. ISBN-13: 978-1439844502., *Exp. Agric.*, 48(2), 305–306,  
1110 2012.

1111 O’Sullivan, D., Murray, B. J., Malkin, T. L., Whale, T. F., Umo, N. S., Atkinson, J. D., Price, H. C.,  
1112 Baustian, K. J., Browse, J. and Webb, M. E.: Ice nucleation by fertile soil dusts: relative importance of  
1113 mineral and biogenic components, *Atmos. Chem. Phys.*, 14(4), 1853–1867, doi:10.5194/acp-14-1853-  
1114 2014, 2014.

1115 O’Sullivan, D., Adams, M. P., Tarn, M. D., Harrison, A. D., Vergara-Temprado, J., Porter, G. C. E.,  
1116 Holden, M. A., Sanchez-Marroquin, A., Carotenuto, F., Whale, T. F., McQuaid, J. B., Walshaw, R.,  
1117 Hedges, D. H. P., Burke, I. T., Cui, Z. and Murray, B. J.: Contributions of biogenic material to the  
1118 atmospheric ice-nucleating particle population in North Western Europe, *Sci. Rep.*, 8(1), 13821,  
1119 doi:10.1038/s41598-018-31981-7, 2018.

1120 Paramonov, M., David, R. O., Kretzschmar, R. and Kanji, Z. A.: A laboratory investigation of the ice  
1121 nucleation efficiency of three types of mineral and soil dust, *Atmos. Chem. Phys.*, 18(22), 16515–16536,  
1122 doi:10.5194/acp-18-16515-2018, 2018.

1123 Van Pelt, R. S. and Zobeck, T. M.: Chemical Constituents of Fugitive Dust, *Environ. Monit. Assess.*,  
1124 130(1), 3–16, doi:10.1007/s10661-006-9446-8, 2007.

1125 Perkins, R. J., Gillette, S. M., Hill, T. C. J. and DeMott, P. J.: The Labile Nature of Ice Nucleation by  
1126 Arizona Test Dust, *ACS Earth Sp. Chem.*, 4(1), 133–141, doi:10.1021/acsearthspacechem.9b00304,  
1127 2020.

1128 Pfannerstill, E. Y., Wang, N., Edtbauer, A., Bourtsoukidis, E., Crowley, J. N., Dienhart, D., Eger, P. G.,  
1129 Ernle, L., Fischer, H., Hottmann, B., Paris, J.-D., Stöner, C., Tadic, I., Walter, D., Lelieveld, J. and  
1130 Williams, J.: Shipborne measurements of total OH reactivity around the Arabian Peninsula and its role in  
1131 ozone chemistry, *Atmos. Chem. Phys.*, 19(17), 11501–11523, doi:10.5194/acp-19-11501-2019, 2019.

1132 Price, H. C., Baustian, K. J., McQuaid, J. B., Blyth, A., Bower, K. N., Choularton, T., Cotton, R. J., Cui,  
1133 Z., Field, P. R., Gallagher, M., Hawker, R., Merrington, A., Miltenberger, A., Neely III, R. R., Parker, S.  
1134 T., Rosenberg, P. D., Taylor, J. W., Trembath, J., Vergara-Temprado, J., Whale, T. F., Wilson, T. W.,  
1135 Young, G. and Murray, B. J.: Atmospheric Ice-Nucleating Particles in the Dusty Tropical Atlantic, *J.*  
1136 *Geophys. Res. Atmos.*, 123(4), 2175–2193, doi:https://doi.org/10.1002/2017JD027560, 2018.

1137 Prodi, F., Santachiara, G. and Olivosi, F.: Characterization of aerosols in marine environments  
1138 (Mediterranean, Red Sea, and Indian Ocean), *J. Geophys. Res. Ocean.*, 88(C15), 10957–10968,  
1139 doi:https://doi.org/10.1029/JC088iC15p10957, 1983.

1140 Rienecker, M. M., Suarez, M. J., Gelaro, R., Todling, R., Bacmeister, J., Liu, E., Bosilovich, M. G.,  
1141 Schubert, S. D., Takacs, L., Kim, G.-K., Bloom, S., Chen, J., Collins, D., Conaty, A., da Silva, A., Gu,  
1142 W., Joiner, J., Koster, R. D., Lucchesi, R., Molod, A., Owens, T., Pawson, S., Pegion, P., Redder, C. R.,  
1143 Reichle, R., Robertson, F. R., Ruddick, A. G., Sienkiewicz, M. and Woollen, J.: MERRA: NASA's  
1144 Modern-Era Retrospective Analysis for Research and Applications, *J. Clim.*, 24(14), 3624–3648,  
1145 doi:10.1175/JCLI-D-11-00015.1, 2011.

1146 Salam, A., Lohmann, U. and Lesins, G.: Ice nucleation of ammonia gas exposed montmorillonite mineral  
1147 dust particles, *Atmos. Chem. Phys.*, 7(14), 3923–3931, doi:10.5194/acp-7-3923-2007, 2007.

1148 Schnell, R. C.: Ice Nuclei in Seawater, Fog Water and Marine Air off the Coast of Nova Scotia: Summer  
1149 1975, *J. Atmos. Sci.*, 34(8), 1299–1305, doi:10.1175/1520-0469(1977)034<1299:INISFW>2.0.CO;2,  
1150 1977.

1151 Schrod, J., Weber, D., Drücke, J., Keleshis, C., Pikridas, M., Ebert, M., Cvetković, B., Nickovic, S.,  
1152 Marinou, E., Baars, H., Ansmann, A., Vrekoussis, M., Mihalopoulos, N., Sciare, J., Curtius, J. and  
1153 Bingemer, H. G.: Ice nucleating particles over the Eastern Mediterranean measured by unmanned aircraft  
1154 systems, *Atmos. Chem. Phys.*, 17(7), 4817–4835, doi:10.5194/acp-17-4817-2017, 2017.

1155 Shahsavani, A., Naddafi, K., Jafarzade Haghighifard, N., Mesdaghinia, A., Yunesian, M., Nabizadeh, R.,  
1156 Arahami, M., Sowlat, M. H., Yarahmadi, M., Saki, H., Alimohamadi, M., Nazmara, S., Motevalian, S. A.  
1157 and Goudarzi, G.: The evaluation of PM<sub>10</sub>, PM<sub>2.5</sub>, and PM<sub>1</sub> concentrations during the Middle Eastern  
1158 Dust (MED) events in Ahvaz, Iran, from april through september 2010, *J. Arid Environ.*, 77, 72–83,  
1159 doi:<https://doi.org/10.1016/j.jaridenv.2011.09.007>, 2012.

1160 Sullivan, R. C., Guazzotti, S. A., Sodeman, D. A. and Prather, K. A.: Direct observations of the  
1161 atmospheric processing of Asian mineral dust, *Atmos. Chem. Phys.*, 7(5), 1213–1236, doi:10.5194/acp-7-  
1162 1213-2007, 2007.

1163 Sullivan, R. C., Miñambres, L., DeMott, P. J., Prenni, A. J., Carrico, C. M., Levin, E. J. T. and  
1164 Kreidenweis, S. M.: Chemical processing does not always impair heterogeneous ice nucleation of mineral  
1165 dust particles, *Geophys. Res. Lett.*, 37(24), doi:<https://doi.org/10.1029/2010GL045540>, 2010a.

1166 Sullivan, R. C., Petters, M. D., DeMott, P. J., Kreidenweis, S. M., Wex, H., Niedermeier, D., Hartmann,  
1167 S., Clauss, T., Stratmann, F., Reitz, P., Schneider, J. and Sierau, B.: Irreversible loss of ice nucleation  
1168 active sites in mineral dust particles caused by sulphuric acid condensation, *Atmos. Chem. Phys.*, 10(23),  
1169 11471–11487, doi:10.5194/acp-10-11471-2010, 2010b.

1170 Suski, K. J., Hill, T. C. J., Levin, E. J. T., Miller, A., DeMott, P. J. and Kreidenweis, S. M.: Agricultural  
1171 harvesting emissions of ice-nucleating particles, *Atmos. Chem. Phys.*, 18(18), 13755–13771,  
1172 doi:10.5194/acp-18-13755-2018, 2018.

1173 Tadic, I., Crowley, J. N., Dienhart, D., Eger, P., Harder, H., Hottmann, B., Martinez, M., Parchatka, U.,  
1174 Paris, J.-D., Pozzer, A., Rohloff, R., Schuladen, J., Shenolikar, J., Tauer, S., Lelieveld, J. and Fischer, H.:  
1175 Net ozone production and its relationship to nitrogen oxides and volatile organic compounds in the  
1176 marine boundary layer around the Arabian Peninsula, *Atmos. Chem. Phys.*, 20(11), 6769–6787,  
1177 doi:10.5194/acp-20-6769-2020, 2020.

1178 Tobo, Y., DeMott, P. J., Hill, T. C. J., Prenni, A. J., Swoboda-Colberg, N. G., Franc, G. D. and  
1179 Kreidenweis, S. M.: Organic matter matters for ice nuclei of agricultural soil origin, *Atmos. Chem. Phys.*,  
1180 14(16), 8521–8531, doi:10.5194/acp-14-8521-2014, 2014.

1181 Ullrich, R., Hoose, C., Möhler, O., Niemand, M., Wagner, R., Höhler, K., Hiranuma, N., Saathoff, H. and

1182 Leisner, T.: A new ice nucleation active site parameterization for desert dust and soot, *J. Atmos. Sci.*,  
1183 74(3), 699–717, doi:10.1175/JAS-D-16-0074.1, 2017.

1184 Vali, G.: Quantitative Evaluation of Experimental Results on the Heterogeneous Freezing Nucleation of  
1185 Supercooled Liquids, *J. Atmos. Sci.*, 28(3), 402–409, doi:10.1175/1520-  
1186 0469(1971)028<0402:QEOERA>2.0.CO;2, 1971.

1187 Vergara-Temprado, J., Murray, B. J., Wilson, T. W., O’Sullivan, D., Browse, J., Pringle, K. J., Ardon-  
1188 Dryer, K., Bertram, A. K., Burrows, S. M., Ceburnis, D., Demott, P. J., Mason, R. H., O’Dowd, C. D.,  
1189 Rinaldi, M. and Carslaw, K. S.: Contribution of feldspar and marine organic aerosols to global ice  
1190 nucleating particle concentrations, *Atmos. Chem. Phys.*, 17(5), 3637–3658, doi:10.5194/acp-17-3637-  
1191 2017, 2017.

1192 Vergara-Temprado, J., Miltenberger, A. K., Furtado, K., Grosvenor, D. P., Shipway, B. J., Hill, A. A.,  
1193 Wilkinson, J. M., Field, P. R., Murray, B. J. and Carslaw, K. S.: Strong control of Southern Ocean cloud  
1194 reflectivity by ice-nucleating particles, *Proc. Natl. Acad. Sci.*, 115(11), 2687 LP – 2692,  
1195 doi:10.1073/pnas.1721627115, 2018.

1196 Wang, N., Edtbauer, A., Stönnner, C., Pozzer, A., Bourtsoukidis, E., Ernle, L., Dienhart, D., Hottmann, B.,  
1197 Fischer, H., Schuladen, J., Crowley, J. N., Paris, J.-D., Lelieveld, J. and Williams, J.: Measurements of  
1198 carbonyl compounds around the Arabian Peninsula: overview and model comparison, *Atmos. Chem.*  
1199 *Phys.*, 20(18), 10807–10829, doi:10.5194/acp-20-10807-2020, 2020.

1200 Wang, X., Deane, G. B., Moore, K. A., Ryder, O. S., Stokes, M. D., Beall, C. M., Collins, D. B.,  
1201 Santander, M. V, Burrows, S. M., Sultana, C. M. and Prather, K. A.: The role of jet and film drops in  
1202 controlling the mixing state of submicron sea spray aerosol particles, *Proc. Natl. Acad. Sci.*, 114(27),  
1203 6978–6983, doi:10.1073/pnas.1702420114, 2017.

1204 von der Weiden, S.-L., Drewnick, F. and Borrmann, S.: Particle Loss Calculator – a new software tool for  
1205 the assessment of the performance of aerosol inlet systems, *Atmos. Meas. Tech.*, 2(2), 479–494,  
1206 doi:10.5194/amt-2-479-2009, 2009.

1207 Welti, A., Lüönd, F., Kanji, Z. A., Stetzer, O. and Lohmann, U.: Time dependence of immersion freezing:  
1208 an experimental study on size selected kaolinite particles, *Atmos. Chem. Phys.*, 12(20), 9893–9907,  
1209 doi:10.5194/acp-12-9893-2012, 2012.

1210 Wex, H., DeMott, P. J., Tobo, Y., Hartmann, S., Rösch, M., Clauss, T., Tomsche, L., Niedermeier, D. and  
1211 Stratmann, F.: Kaolinite particles as ice nuclei: learning from the use of different kaolinite samples and  
1212 different coatings, *Atmos. Chem. Phys.*, 14(11), 5529–5546, doi:10.5194/acp-14-5529-2014, 2014.

1213 Wex, H., Huang, L., Zhang, W., Hung, H., Traversi, R., Becagli, S., Sheesley, R. J., Moffett, C. E.,  
1214 Barrett, T. E., Bossi, R., Skov, H., Hünerbein, A., Lubitz, J., Löffler, M., Linke, O., Hartmann, M.,  
1215 Herenz, P. and Stratmann, F.: Annual variability of ice-nucleating particle concentrations at different  
1216 Arctic locations, *Atmos. Chem. Phys.*, 19(7), 5293–5311, doi:10.5194/acp-19-5293-2019, 2019.

1217 Whale, T. F., Murray, B. J., O’Sullivan, D., Wilson, T. W., Umo, N. S., Baustian, K. J., Atkinson, J. D.,  
1218 Workneh, D. A. and Morris, G. J.: A technique for quantifying heterogeneous ice nucleation in microlitre  
1219 supercooled water droplets, *Atmos. Meas. Tech.*, 8(6), 2437–2447, doi:10.5194/amt-8-2437-2015, 2015.

1220 Wilson, T. W., Ladino, L. a., Alpert, P. a., Breckels, M. N., Brooks, I. M., Browse, J., Burrows, S. M.,  
1221 Carslaw, K. S., Huffman, J. A., Judd, C., Kilhau, W. P., Mason, R. H., McFiggans, G., Miller, L. a.,  
1222 Nájera, J. J., Polishchuk, E., Rae, S., Schiller, C. L., Si, M., Temprado, J. V., Whale, T. F., Wong, J. P. S.,  
1223 Wurl, O., Yakobi-Hancock, J. D., Abbatt, J. P. D., Aller, J. Y., Bertram, A. K., Knopf, D. a. and Murray,  
1224 B. J.: A marine biogenic source of atmospheric ice-nucleating particles, *Nature*, 525(7568), 234–238,  
1225 doi:10.1038/nature14986, 2015.

1226 Wu, W.-S., Purser, R. J. and Parrish, D. F.: Three-Dimensional Variational Analysis with Spatially  
1227 Inhomogeneous Covariances, *Mon. Weather Rev.*, 130(12), 2905–2916, doi:10.1175/1520-  
1228 0493(2002)130<2905:TDVAWS>2.0.CO;2, 2002.

1229 Yadav, S., Venezia, R. E., Paerl, R. W. and Petters, M. D.: Characterization of Ice-Nucleating Particles  
1230 Over Northern India, *J. Geophys. Res. Atmos.*, 124(19), 10467–10482,  
1231 doi:https://doi.org/10.1029/2019JD030702, 2019.

1232 Yahya, R. Z., Arrieta, J. M., Cusack, M. and Duarte, C. M.: Airborne Prokaryote and Virus Abundance  
1233 Over the Red Sea, *Front. Microbiol.*, 10, 1112, doi:10.3389/fmicb.2019.01112, 2019.

1234 Yang, J., Wang, Z., Heymsfield, A. J., DeMott, P. J., Twohy, C. H., Suski, K. J. and Toohey, D. W.: High  
1235 ice concentration observed in tropical maritime stratiform mixed-phase clouds with top temperatures  
1236 warmer than  $-8^{\circ}\text{C}$ , *Atmos. Res.*, 233, 104719, doi:https://doi.org/10.1016/j.atmosres.2019.104719, 2020.

1237 Yost, J. L. and Hartemink, A. E.: Chapter Four - Soil organic carbon in sandy soils: A review, vol. 158,  
1238 edited by D. L. Sparks, pp. 217–310, Academic Press., 2019.

1239 Yu, Y., Kalashnikova, O. V, Garay, M. J., Lee, H. and Notaro, M.: Identification and Characterization of  
1240 Dust Source Regions Across North Africa and the Middle East Using MISR Satellite Observations,  
1241 *Geophys. Res. Lett.*, 45(13), 6690–6701, doi:https://doi.org/10.1029/2018GL078324, 2018.

1242 Zolles, T., Burkart, J., Häusler, T., Pummer, B., Hitzenberger, R. and Grothe, H.: Identification of Ice

1243 Nucleation Active Sites on Feldspar Dust Particles, *J. Phys. Chem. A*, 119(11), 2692–2700,  
1244 doi:10.1021/jp509839x, 2015.  
1245